



MMP-12 siRNA improves the homeostasis of the small intestine and metabolic dysfunction in high-fat diet feeding-induced obese mice

Mingming Song^a, Shiyao Zhang^a, Zixuan Tao^a, Jianning Li^b, Yujie Shi^c, Yonghong Xiong^a, Wenxiang Zhang^a, Chang Liu^a, Siyu Chen^{a,*}

^a State Key Laboratory of Natural Medicines and School of Life Science and Technology, China Pharmaceutical University, Nanjing, 211198, PR China

^b Nanjing Qixia Hospital, Nanjing, 210046, PR China

^c Women's Hospital of Nanjing Medical University, Nanjing Maternity and Child Health Care Hospital, Nanjing, 210004, PR China

ARTICLE INFO

Keywords:

Obesity
Matrix metalloprotein-12
Drug delivery system
Small intestinal microenvironments
Nuclear factors

ABSTRACT

The changes of small intestinal homeostasis have been recognized to contribute essentially to the obese development. However, the core small intestinal regulator which mediates over-nutrient impacts on the homeostasis of the small intestines remains elusive. Here, we identify the MMP-12 as such a responsive factor in mouse small intestines. Taking advantages of the nano delivery system, we demonstrate that small intestine-specific MMP-12 knockdown alleviates high-fat diet feeding-induced metabolic disorders and improves intestinal homeostasis in mice, including a significant decrease in lipid transportation, bile acid reabsorption, and inflammation. In parallel, the small intestinal integrity is recovered and the gut microbiota composition is reversed towards that under normal diet feeding. Mechanistically, MMP-12, differing from its traditional elastolytic function, acts as a transcriptional factor to activate *Fabp4* transcription through epigenetic modification. In translational medicine, clinical applications of our nanosystem and therapeutic interventions targeting MMP-12 will benefit patients with obesity and associated diseases.

1. Introduction

With the development of the global social economy in the 21st century, obesity has become a global pandemic disease [1,2]. Over the last 40 years, the prevalence of obesity has almost tripled worldwide [3]. The development of obesity is closely associated with multiple diseases, such as type 2 diabetes, hepatic steatosis, cardiovascular diseases, and even cancer [4–9]. Hence, obesity is a great threat to public health and causes an economic burden for society. Although effective strategies, including lifestyle intervention, conventional pharmacology and weight-loss surgery, are well established to counteract obesity, their undesirable inconstancy and side effects are not exempt in all cases [7, 10]. Therefore, an urgent medical need exists for the large and heterogeneous population of obese patients.

Although obesity is caused by various pathological factors, changes in the small intestinal homeostasis have been recognized to contribute essentially to obesity progression [11]. As the first organ exposed to nutrients, the small intestine has to change its capacity to adapt external nutrient signals, such as a HFD [12]. When challenged with dietary fat,

our stomach functions as a bioreactor for dietary lipid oxidation. These lipids are further engulfed by enterocytes within the duodenum and are re-esterified into complex lipid molecules [4]. Then, they bind with lipoproteins (e.g., ApoB48 and ApoB100) and are assembled into primarily chylomicrons in the jejunum [13]. These chylomicrons enter the lymphatics through lacteals and further drain into the venous circulation [14,15]. Subsequently, the ileum plays a nonredundant role in handling lipid overflow by controlling bile acid (BA) reabsorption, cholesterol absorption and metabolism [16–18]. In addition, disruptions of lipid homeostasis can lead to unexpected intestinal inflammation and permeability destruction, as well as alterations in the composition of the intestinal microbiota [19–21]. Collectively, the coordination of such processes in the whole intestine guarantees metabolic homeostasis within our bodies. However, diets with high fat have been associated with various metabolic syndromes, including obesity and diabetes mellitus [22]. These HFD feeding-induced detrimental effects are ascribed to their profound impacts on the overall intestinal homeostasis as stated above. Thus, correction of the small intestinal homeostasis has become a promising approach to treat obesity.

* Corresponding author.

E-mail address: siyuchen@cpu.edu.cn (S. Chen).

<https://doi.org/10.1016/j.biomaterials.2021.121183>

Received 2 March 2021; Received in revised form 1 October 2021; Accepted 7 October 2021

Available online 11 October 2021

0142-9612/© 2021 The Authors.

Published by Elsevier Ltd.

This is an open access article under the CC BY-NC-ND license

(<http://creativecommons.org/licenses/by-nc-nd/4.0/>).

To screen out the direct mediator that transfers HFD signals to intestinal homeostasis, we clustered high-throughput RNA-seq results from the jejunum and ileum (two major organs for lipid absorption) collected from mice subjected to 11 weeks of HFD feeding. We found that the mRNA expression levels of MMP-12 were markedly elevated in both small intestinal tissues. MMP-12 was first demonstrated as an inflammatory macrophage-secreted elastolytic MMP [23]. In addition, MMP-12 is able to degrade a broad spectrum of extracellular matrix (ECM) components, such as collagen IV, fibronectin and laminin. Hence, inflammation-induced MMP-12 degrades the basement membrane, allowing macrophages to penetrate into injured tissue [24]. Accordingly, the expression and enzymatic activity of MMP-12 are increased in multiple inflammatory diseases, including atherosclerosis and chronic obstructive pulmonary disease [25]. Importantly, MMP-12 is involved in obesity development. For example, MMP-12 is highly expressed in the adipose tissue of HFD-fed mice. MMP-12 deficiency alleviates obesity-induced inflammation and improves metabolic dysfunction. Such a beneficial effect may be dependent on the organization and composition of the ECM, raising the possibility that MMP-12-orchestrated ECM deposition and degradation are involved in maintaining metabolic homeostasis. Notably, intestinal ECM homeostasis is abolished in HFD-fed mice. Hence, identification of the role of MMP-12 in the regulation of small intestinal function is of great urgency in the treatment of obesity.

In the present study, to effectively and specifically knock down MMP-12 in mouse small intestines, we established a new nanoparticle (NP) system consisting of chitosan (CS), PLGA (poly(lactic-co-glycolic acid)) and polyethylene glycol (PEG) (CS@PLGA NPs, CPA NPs) to specifically deliver MMP-12 siRNAs into mouse small intestines. By making the best of this NPs system, we found that it improved the small intestinal homeostasis of HFD feeding-induced obese mice. As a consequence, these mice exhibited improved metabolic physiology and reduced systemic inflammation. Mechanistically, MMP-12 exerted DNA-binding abilities, rather than its elastolytic activity, to induce fatty acid-binding protein 4 (*Fabp4*) transcription. Taken together, we demonstrated a mediatory role of MMP-12 in transferring HFD signals to small intestinal homeostasis and systemic metabolic homeostasis.

2. Materials and methods

2.1. Animals

Male C57BL/6 J mice were purchased from the Model Animal Research Center of Nanjing University (Nanjing, Jiangsu, China). Male C57BL/6 J mice were maintained in a 12 h LD cycle and in a temperature- and humidity-controlled environment. Note that we housed these mice at a thermoneutral temperature (26 ± 1 °C) to avoid the mild cold (22 ± 1 °C)-induced activation impacts on the energy expenditure of mice. All experiments were approved and conducted according to the guidance of the Laboratory Animal Care & Use Committee at China Pharmaceutical University (Permit number SYXK-2016-0011). To establish the HFD-fed obese model, 10-week-old mice were fed with HFD (60% kcal from fat, Research Diets, New Brunswick, NJ, USA) for 11 weeks. To dissect the role of MMP-12 in the regulation of intestinal homeostasis, MMP-12 expression was knocked down in the mouse small intestine by using CPA NPs carrying either a MMP-12 siRNA mixture (at a dose of 40 µg/kg body weight once every 3 days) or its corresponding control for a total of 27 days. The following day after final gavage, mice were analyzed and later sacrificed to collect sera, tissues and feces for further analyses.

2.2. Cell culture

Caco-2 cell line was obtained from the Cell Bank of the Chinese Academy of Sciences (Shanghai, China). Cells were cultured in Dulbecco's modification of Eagle's medium (DMEM, Gibco, Waltham, MA,

USA) supplemented with 10% fetal bovine serum (FBS, ScienCell, San Diego, CA, USA) with 1% antibiotics (penicillin/streptomycin, Sigma, Louis, MO, USA) at 37 °C in a humidified atmosphere containing 5% CO₂.

2.3. Human subjects

Human serum and fecal samples were freshly isolated from control and hyperlipidemic persons (serum triglycerides (TG) levels ranging from 0.78 to 2.68 mmol/L and serum total cholesterol (TC) levels ranging from 3.86 to 6.33 mmol/L). Pearson correlation analysis was performed to examine the correlation of fecal MMP-12 levels with serum TG or TC. This study was approved by the Ethics Committee at Nanjing Qixia Hospital (Permit number 20191202), all patients have written the informed consent.

2.4. High-throughput RNA sequencing

To screen candidates in mouse small intestines that linking HFD signals to the lipid homeostasis, mice were fed with HFD for 11 weeks, as described above. Small intestine (ileum and jejunum) samples were pooled and the total RNA was isolated to construct the RNA-seq libraries. The quality of the RNA libraries was evaluated using the Agilent 2100 Bioanalyzer (Agilent Technologies, Palo Alto, CA, USA). Library preparations were sequenced on an Illumina HiSeq platform (Illumina, San Diego, CA, USA) by Novogene Co., LTD. Fragments Per Kilobase of transcript per Million mapped reads (FPKM) were calculated for additional statistics. All reads were mapped to the mouse genome (GRCm38/mm10) [26]. The differentially expressed transcripts of small intestine were analyzed by either DESeq2 (with biological repeat) or edgeR (without biological repeat) package of R software, $P < 0.05$ and $|\text{Log}_2(\text{Fold change})| \geq 2.5$ (only for screening key genes in Fig. 1) or ≥ 1 (for other analyses) were considered to be statistically difference. The visualization of differential gene is performed by ggplot2 package of R software. ClusterProfiler package of R language was used to analyze and visualize GO terms of the differential genes. $P < 0.05$ was considered as a threshold of GO enrichment analysis.

2.5. Gene and protein analyses

The gene mRNA and protein expression are examined as described in our previous study [27]. Note that the gene expression levels were normalized to *36B4* (for mouse tissues) and *β-actin* (for human Caco-2 cells). A complete list of qPCR primers is shown in Table S12. For the protein expression analysis, antibodies against MMP-12 (Cat. No. 22989-1-AP; 1:1000 dilution), ApoB-48 (Cat. No. 20578-1-AP; 1:2000 dilution), ZO-1 (Cat. No. 21773-1-AP; 1:5000 dilution), Occludin (Cat. No. 27260-1-AP; 1:3000 dilution), Fabp1 (Cat. No. 13626-1-AP; 1:2000 dilution), Fabp2 (Cat. No. 21252-1-AP; 1:2000 dilution), Fabp3 (Cat. No. 10676-1-AP; 1:2000 dilution), Fabp4 (Cat. No. 12802-1-AP; 1:2000 dilution), Fabp5 (Cat. No. 12348-1-AP; 1:2000 dilution), Fabp6 (Cat. No. 13781-1-AP; 1:2000 dilution) and Fabp7 (Cat. No. 51010-1-AP; 1:2000 dilution) were purchased from Proteintech (Chicago, IL, USA). The antibody against Fabp12 (Cat. No. A12620; 1:1000 dilution) was purchased from ABclonal Technology Co., Ltd. (Wuhan, Hubei, China). The antibody against β-ACTIN (Cat. No. BS6007MH; 1:1000 dilution) was purchased from Bioworld Technology (Nanjing, Jiangsu, China).

2.6. MMP-12 activity

MMP-12 activity was determined by casein zymography as described before [28]. Additionally, protein concentrations in the mouse jejunum, ileum and Caco-2 cells were determined using the BCA method (Beyotime Biotechnology Company, Shanghai, China). All samples (total protein concentration 10 µg/lane) were separated on 10% gelatin gels. After electrophoresis, gels were stained with 0.25% Coomassie brilliant

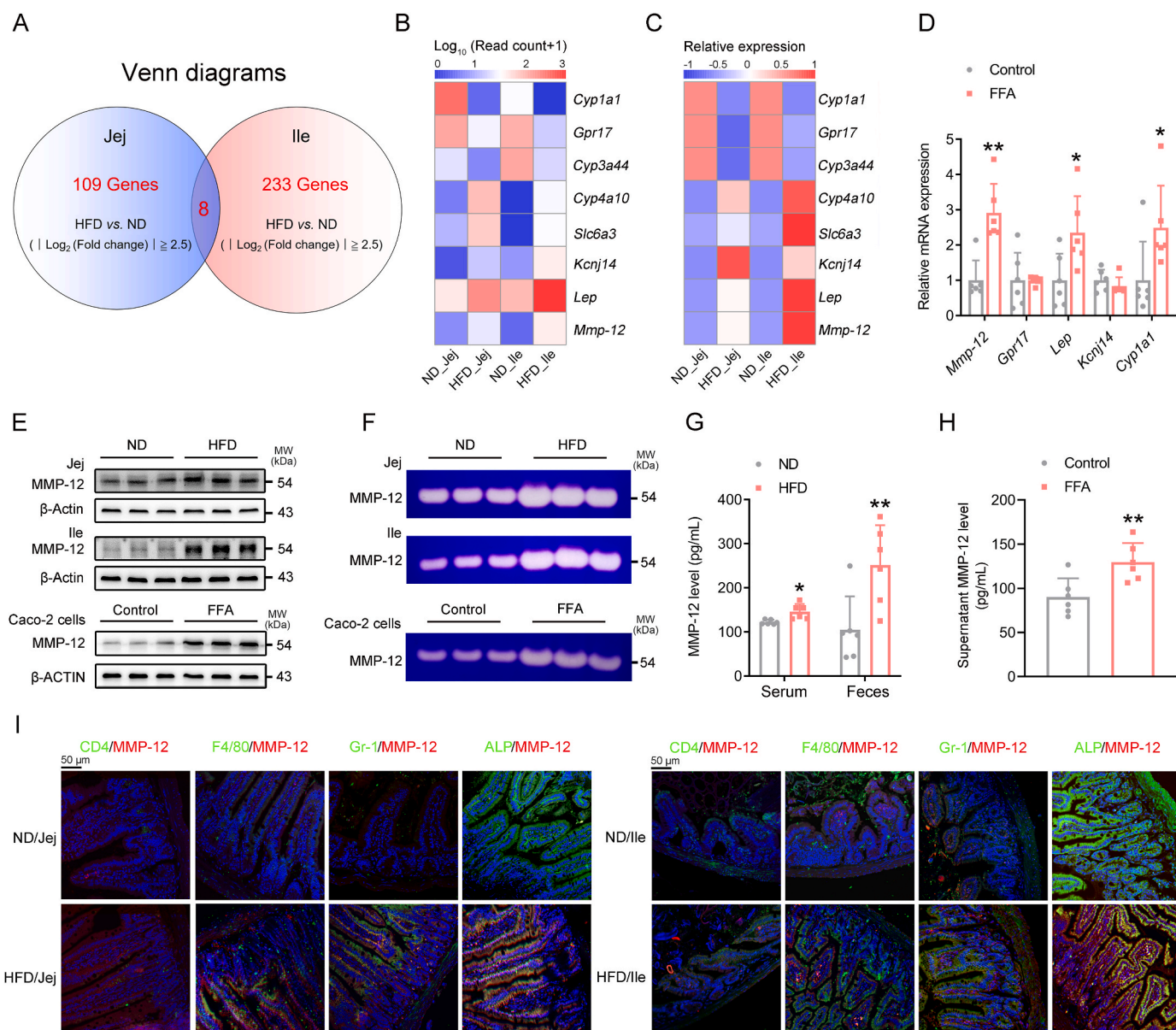


Fig. 1. MMP-12 responses to HFD signals in mouse small intestines. (A) Venn diagrams of high-throughput RNA sequencing results from small intestinal samples (including jejunum and ileum, respectively) of mice fed either an ND or an HFD for 11 weeks. (B) Heat map of eight clustered genes derived from high-throughput RNA sequencing results. (C) RT-qPCR validation of eight clustered gene mRNA expression levels in the small intestine of HFD-fed mice, $N = 6$ for each group. (D) RT-qPCR analyses of mRNA expression levels of 5 genes in Caco-2 cells treated with 0.4 mM FFAs for 24 h $*P < 0.05$, $**P < 0.01$ vs. control group, $N = 6$ for each group. (E) Western blot analysis of MMP-12 protein expression levels in the small intestines of HFD-fed mice (upper) and FFA-treated Caco-2 cells (below). (F) Zymographic analysis of MMP-12 enzymatic activity in the small intestines of HFD-fed mice (upper) and FFA-treated Caco-2 cells (below). (G) Serum and fecal MMP-12 levels in HFD-fed mice. $*P < 0.05$, $**P < 0.01$ vs. ND group, $N = 6$ for each group. (H) Supernatant MMP-12 levels in FFA-treated Caco-2 cells. $*P < 0.05$, $**P < 0.01$ vs. Control group, $N = 6$ for each group. (I) IF analysis of the small intestinal protein expression levels of MMP-12 accompanied with CD4, Gr-1, F4/80 and ALP (scale bars: 50 μm). Quantitative data were presented as mean \pm SD. Significance was assessed using two-tailed Student's *t*-test. Jej: jejunum; Ile: ileum.

blue R-250 and then incubated in the eluent (10% acetic acid, 20% methanol in distilled water) until bands of gelatinolytic activity were visualized.

2.7. Synthesis and characterizations of CPA NPs

CPA NPs were synthesized by two-step reactions. Firstly, the PLGA NPs were prepared using a nanoprecipitation method [29]. In brief, 10 mg of PLGA-PEG polymer was dissolved in 1 mL of acetone to form a primary emulsion which was further emulsified in an aqueous polyvinyl alcohol (PVA) solution (12 mL, 2% w/v) to form an oil-in-water emulsion using a probe sonicator for 30 s at 180 W over an ice bath. Then, the

solution was dropped into 25 mL of deionized water and stirred for 1.5 h to allow solvent evaporation. The NPs suspension was then rinsed 3 times by centrifugation (12,000 rpm, 4 $^{\circ}\text{C}$, 15 min) and dispersed in water by stirring for 15 min. The PLGA NPs were used fresh or kept at -80°C for various studies. Secondly, we used a stable self-assembly method to prepare CPA NPs as described previously. A fixed amount of PLGA NPs were suspended in a 0.4% (w/v) sodium tripolyphosphate solution, and slowly added dropwise to a 1% (w/v) CS solution, and continuously stirred at room temperature for 1 h. The suspension was then centrifuged at 14,000 rpm for 15 min at 4 $^{\circ}\text{C}$, and the supernatant was removed. It was then washed twice with deionized water, and the NPs recovered by centrifugation were resuspended in buffer for further

use. CPA NPs containing GM6001 (a well-known MMP-12 inhibitor) or MMP-12 siRNA were synthesized using the above method. Furthermore, the amount of GM6001 and siRNA loaded into the NPs were analyzed by ultraviolet spectrophotometer (UV-1800 PC, Mapada Instruments Limited, Shanghai, China). GM6001 or siRNA entrapment efficiency is the ratio of initial drug or RNA contents to that is encapsulated by the NPs. Mean particle size and zeta potential of the prepared NPs with or without CS coating were determined using a Malvern Zetasizer (ZEN3690, Malvern Instruments Limited, Malvern, Worcestershire, UK). Also, nanocarrier were stained with 1% phosphotungstic acid solution and observed for size and morphology using a transmission electron microscopy (TEM) (HT-7700, Hitachi, Tokyo, Japan) operating at 200 kV.

2.8. Nanocarrier stability

To evaluate the nanocarrier stability over time under physiological conditions, CPA NPs were incubated in simulated gastric fluid and simulated intestinal fluid, respectively, and the change in the average particle size and PDI of the NPs was analyzed for 5 h. These characterizations were examined using a Malvern Zetasizer system (ZEN3690, Malvern Instruments Limited, Malvern, Worcestershire, UK) at room temperature.

2.9. Mechanism of cellular uptake of CPA NPs

Caco-2 cells were seeded in 22 mm confocal dishes at a density of 1×10^4 cells per well. Free FAM siRNA and FAM siRNA NPs (NPs: PLGA NPs and CPA NPs) were added to the cells and incubated for 4 h, respectively. Then, cells were washed to remove non-internalized particles, fixed with 4% formaldehyde and nuclei were stained with 4',6-diamidino-2-phenylindole (DAPI). The process of cellular uptake was observed with a Nikon fluorescence microscope (ECLIPSE, Ts2R-FL, Tokyo, Japan). To further identify the mechanism of cellular uptake of CPA NPs, Caco-2 cells were planted in confocal dish as described above. The cells were then pre-incubated for 2 h with serum-free medium containing endocytosis inhibitors. The doses for these inhibitor were selected according to a previous study [30]. The dose of CPZ was 10 $\mu\text{g}/\text{mL}$, the dose of Filipin was 1 $\mu\text{g}/\text{mL}$, and the dose of EIPA was 10 $\mu\text{g}/\text{mL}$. Then, the culture media were removed and replaced with fresh media containing FAM siRNA/CPA NPs for 4 h. Finally, intracellular FAM fluorescence was visualized under a Nikon fluorescence microscope (ECLIPSE, Ts2R-FL, Tokyo, Japan).

2.10. Metabolic cage and insulin sensitivity analyses

Body weights were recorded every week. For food intake measurement, food consumption was weighed once every 3 days for 27 consecutive days. For the metabolic cage study, mice were acclimated in metabolic cages (TSE Systems, Berlin Germany) for 3 days, and then the VO_2 , VCO_2 , and energy expenditure were recorded continuously for another 3 days. The heat production was calculated and adjusted to body weight. To assess the impact of small intestine-specific MMP-12 knockdown on mouse glucose tolerance and insulin sensitivity, Glucose tolerance test (GTT) and insulin tolerance test (ITT) were performed. For the GTT analysis, mice were fasted for 16 h and then injected intraperitoneal (*i.p.*) with glucose (1 g/kg body weight). For ITT analysis, mice were fasted for 6 h and *i.p.* injected with insulin (2 U/kg body weight) [31]. Blood glucose levels were measured before the injection and 15, 30, 60, 120 min after the injection with a glucose monitor (Roche Diagnostics, Indianapolis, IN, USA). Areas under curve (AUC) were calculated and statistically analyzed by Origin8 (Version 8.6, OriginLab, Northampton, MA, USA). Given that the HOMA was used to quantify HOMA-IR. HOMA-IR values were then calculated using fasted glucose and serum insulin values in the following equation: $\text{HOMA-IR} = \text{fasting glucose (mg/dL)} \times \text{fasting insulin (mIU/L)}/405$ [32].

2.11. Serological analysis

Serum samples were collected in a centrifuge tube and centrifuged at 4000 rpm for 10 min at 4 °C. Serum levels of alanine aminotransferase (ALT), aspartate transaminase (AST), TG, TC, low density lipoprotein cholesterol (LDL-C), high density lipoprotein cholesterol (HDL-C), BA, blood urea nitrogen (BUN), creatine, and nonesterified fatty acids (NEFAs), as well as inflammatory cytokines including MCP-1, TNF- α and IL-6 were determined by using commercial kits (Jiancheng Institute of Biotechnology, Nanjing, Jiangsu, China). Serum levels of lipopolysaccharide (LPS) and D-lactitol (D-Lac) were measured with by ELISA assay according to instruction of the manufacturer (Jiancheng Institute of Biotechnology, Nanjing, Jiangsu, China). Serum and fecal MMP-12 levels were measured using the MMP-12 ELISA kit (Ruixin Biotech, Quanzhou, Fujian, China).

2.12. TEM analysis

The TEM analysis was performed by Servicebio company (Wuhan, Hubei, China) according to a previous study [12]. Images were taken by using Hitachi HT7800 electron microscope (HT-7800, Hitachi, Tokyo, Japan).

2.13. Short chain fatty acid (SCFA) analysis

Quantification analysis of fecal SCFAs, including acetic acid, propionic acid, butyric acid, isobutyric acid, valeric acid, and isovaleric acid, were performed on an Agilent 7890 A gas chromatography equipped with an Agilent 5975C mass spectrometric detector. To this end, 100 μg of fecal samples was added to a microfuge tube containing 1 mL of 0.5% H_3PO_4 , then homogenized for 2 min, centrifuged at $17,949 \times g$ for 10 min. Then 800 μL of supernatant was extracted with equal amounts of ethyl acetate and allowed to vortex for 2 min. Samples were centrifuged at $17,949 \times g$ for 10 min. The internal standard of 4-methylpentanoic acid was spiked into the supernatant, and transferred to a gas chromatograph vial. Concentrations of individual SCFAs were analyzed with a polar TG-WAS capillary column (30 mm \times 0.25 mm \times 0.25 μm , Thermo, Waltham, MA, USA). Helium was used as a carrier gas at a constant flow rate of 1 mL/min. The injector temperature was 280 °C and the ion source temperature was 280 °C. The initial oven temperature was 80 °C, rising to 200 °C at 10 °C/min, then to 225 °C at 5 °C/min, and finally to 250 °C at a rate of 2 °C/min, with a final hold at this temperature for 5 min.

2.14. Transfection and reporter gene assays

Promoter activity assays were conducted in Caco-2 cells. The human *FABP4* promoter (−200 to −1 bp) was amplified from the human genomic DNA by using primers shown in Table S12. The poly(A) tract of the MMP-12 binding sites were mutated and synthesized by Tsingke company (Nanjing, Jiangsu, China). All transient transfections were conducted as previously described [33].

2.15. ChIP assay

ChIP assays were performed in Caco-2 cells with/without MMP-12 overexpression as previously described [33]. For the antibody information, the anti-MMP-12 (Cat. No. ab52897, Abcam, Cambridge, MA, USA) and anti-Ach3 (Cat. No. 06–599, Millipore, Bedford, MA, USA), anti-H3K9–Me2, Cat. No. ab1220, Abcam, Cambridge, MA, USA), or normal mouse IgG (Cat. No. SC-2025, Santa Cruz, Dallas, TX, USA) in the presence of bovine serum albumin (BSA) and salmon sperm DNA. In addition, the qPCR using primers flanking the proximal binding sites for MMP-12 on the human *FABP4* promoter were presented in Table S12.

2.16. Statistical analysis

Statistical analysis was performed by using the GraphPad Prism 7 programme (California, USA). Quantitative data were presented as mean \pm SD. Two-group comparisons were performed using two-tailed Student's *t*-test. Multigroup comparisons were performed using one-way ANOVA followed Tukey's multiple comparisons test. Spearman correlation analysis was performed between SCFAs, gene expression, and operational taxonomic units (OTUs) using psych package of R, and the correlation heatmap was drawn through the heatmap package. A *P* value < 0.05 was considered statistically significant.

3. Results

3.1. MMP-12 responses to HFD signals in mouse small intestines

To address the aforementioned question, we performed high-throughput RNA sequencing by using small intestinal samples (including jejunum and ileum) dissected from 11-week HFD-fed mice. Bioinformatic analysis revealed a cluster of 8 genes that were robustly regulated by HFD signals in both the mouse jejunum and the ileum (Fig. 1A and B, Table S1), which was confirmed by independent RT-qPCR and semiquantitative analyses (Fig. 1C and S1A, Table S2). Moreover, *in vitro* analysis revealed that 0.4 mM free fatty acids (FFAs, an equimolar mixture of oleic acid and palmitic acid) increased the mRNA expression levels of *MMP-12*, *LEP* and *CYP11A1* in Caco-2 cells, a colorectal adenocarcinoma-derived cell line. However, other genes, including *GPR17* and *KCNJ14*, were modestly altered by such stimulation (Fig. 1D). Given that *MMP-12* was the most responsive gene corresponding to the hyperlipidemic signals *in vivo* and *in vitro*, we ultimately focused our research on this gene. Consistently, the protein expression levels of *MMP-12* were similarly increased (Fig. 1E, S1B and S1C).

Of note, *MMP-12* is also a macrophage metal elastase that possesses

biological and pathophysiological functions based on its enzymatic activity. Hence, we evaluated the enzymatic activities of *MMP-12* and found that they were consistently increased in the jejunum and ileum of HFD-fed mice, as well as in FFA-treated Caco-2 cells (Fig. 1F, S1D and S1E). Moreover, *MMP-12* is known as a secretory protease that degrades the ECM during the destruction of inflammatory tissues. As shown in Fig. 1G, the serum and fecal levels of *MMP-12* were correspondingly increased in HFD-fed mice. Meanwhile, FFAs also increased the *MMP-12* concentrations in the supernatant from Caco-2 cells (Fig. 1H). In addition, immunofluorescence (IF) analyses revealed that this HFD-induced *MMP-12* mainly accumulated in ALP-expressing epithelial cells, but not in F4/80-positive macrophages, Gr-1-positive neutrophils, and CD4-positive T lymphocytes (Fig. 1I), indicating *MMP-12* may exert its function in epithelial cells within the small intestines. Taking these data together, we concluded that *MMP-12* may serve as an important factor responding to HFD signals in the small intestine.

3.2. Preparation and characterization of CPA NPs

To specifically and effectively knock down *MMP-12* in the small intestines of HFD-fed mice, we designed an oral NP system using PLGA-PEG and CS based on the pH-sensitive and adhesive effects of CS. In brief, PLGA-PEG was first synthesized by conjugating COOH-PEG-NH₂ to PLGA-N-hydroxysuccinimide (PLGA-NHS) through amide bond formation (Fig. 2A). In the ¹H nuclear magnetic resonance (NMR) spectra of PLGA-PEG, the peaks at 5.2, 4.8, 3.7, and 1.6 ppm were ascribed to (3, -OCH₂-), (2, -OCH₂-), (4, -CH₂-CH₂O-), and (5, -OCH(CH₃)-), respectively (Fig. 2B). The degradable CPA NPs were prepared using PLGA-PEG polymer (as a core) coated with a CS shell (as a protective shelter to avoid gastric acid) by double-emulsion and ionic gelation strategies (Fig. 2C). The CPA NPs were roughly spherical in shape and had a particle diameter of ~227 nm, as analyzed by TEM and light scattering spectrometry (Fig. 2D). The polymer disparity index (PDI) and zeta potential were 0.23 \pm 0.01 and 57.8 \pm 4.98 mV, respectively (Fig. 2E).

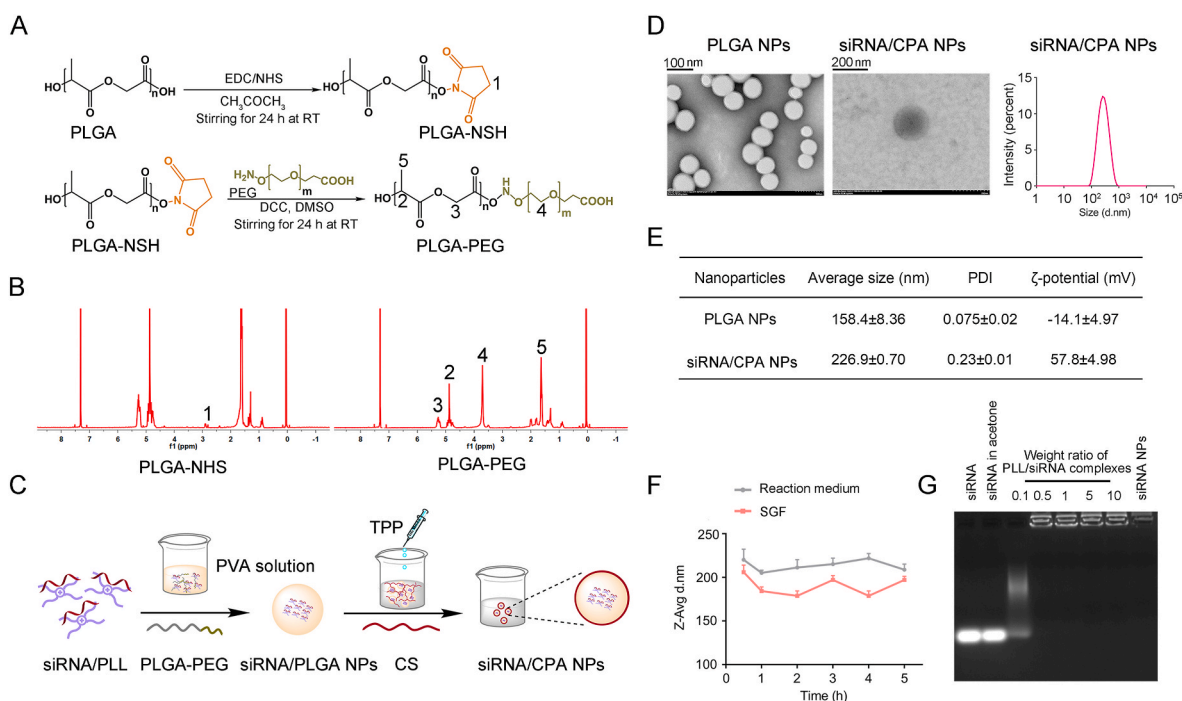


Fig. 2. Preparation and Characterization of CPA NPs. (A) The reaction scheme of PLGA-PEG synthesis. (B) ¹H NMR spectra of PLGA-PEG. (C) Synthesis process of CPA NPs and the schematic representation of particle structure. (D) Representative TEM images of PLGA NPs (scale bars: 100 nm) and CPA NPs (left) (scale bars: 200 nm), size distribution of CPA NPs measured by Mastersizer Micro (right). (E) Zeta-potential of PLGA NPs and CPA NPs. (F) Stability of CPA NPs in the simulated gastric fluid (SGF) for the indicated times, *N* = 3 for each group. (G) Agarose gel electrophoresis assay of siRNA stability in organic solvent, naked or complexed with PLL. Quantitative data were presented as mean \pm SD.

Essential to the NP system, the protonation of the CS shell stabilized the PLGA-PEG NPs under acidic conditions (Fig. 2F). Next, cationic poly-L-lysine (PLL) was used for siRNA complexation (PLL/siRNA weight ratio of 0.5, Fig. 2G). In contrast, this shell collapsed in the simulated intestinal fluid (SIF), an *in vitro* system that mimics the basic environment in the small intestines (Table S3) [34].

Endocytosis has been well recognized as an important process through which extracellular cargos are internalized by cells [35]. To identify the mechanisms through which the CPA NPs entered the intestinal cells, we treated human Caco-2 cells with CPA NPs carrying FAM siRNA (with green fluorescence) for 4 h in the presence of different inhibitors for the endocytic process. As shown in Fig. 3A, CPA NP transfection was partially blocked by treatment with either EIPA (a macropinocytotic inhibitor) or chlorpromazine (a clathrin-mediated endocytic inhibitor). Notably, cellular uptake was dramatically diminished in combination with filipin (a caveolae-mediated endocytic inhibitor). Taken together, these results suggested that caveolae-mediated endocytosis is the predominant pathway for the cellular uptake of CPA NPs. In addition, the CPA NP-coated siRNA was more prone to absorption than the PLGA NPs (Fig. 3B), which could be explained by the stronger positive electricity of the CPA NPs.

To evaluate the biodistribution of CPA NPs, Cy5-siRNA was loaded in PLGA to form fluorescent NPs for *in vivo* tracking. Next, the mice were gavaged with Cy5-siRNA-labeled CPA NPs (40 $\mu\text{g}/\text{kg}$) and equivalent Cy5-siRNA-labeled PLGA NPs for 72 h. We found that the fluorescent signals of Cy5-siRNA-labeled CPA NPs accumulated in mouse small

intestines and exhibited retentive ability compared with that of the Cy5-siRNA-labeled PLGA NPs at 72 h (Fig. 3C). Since the intestine is the main target organ of our CPA NPs, we therefore investigated the fluorescence distribution of Cy5-siRNA in the intestine of mice administrated with either PLGA or CPA NPs at the 48-h time point, and found that each of them was quite non-uniform (Figure S2A). Hence, we extended the time interval and detected the fluorescent signals of Cy5-siRNA at 72-h time point. As shown in Fig. 3D, the Cy5-siRNA-loaded CPA NPs were evenly distributed at this time point. In addition, we did not observe any fluorescent signals in other metabolic organs, including the liver, epididymal white adipose tissue (eWAT), kidney, or spleen (Fig. 3E).

Considering that CPA NPs are possibly circulated in blood after passing enterocytes, serum siRNA levels were further examined at the indicated time points in order to verify off-target effects in other organs. By using fluorescence spectrophotometer analysis, we found that serum Cy5-siRNA levels from CPA NPs-treated mice were significantly lower at each time point, when compared to those from PLGA NPs-treated mice (Figure S2B). These data further demonstrated that CS could function as a shell to preserve the siRNA within the small intestines. Meanwhile, we noticed that Cy5-siRNA was still existed with in the circulation system of CPA NPs-treated mice. Such relative low levels of serum Cy5-siRNA might be caused by the unavoidable free PLGA NPs formed during the synthesis of CPA NPs. Additionally, serum levels of Cy5-siRNA from CPA NPs-treated mice were peaked at 48 h and then gradually declined (Figure S2B). Taken these data together, we gavaged the mice with the CPA NPs in a 3-day interval.

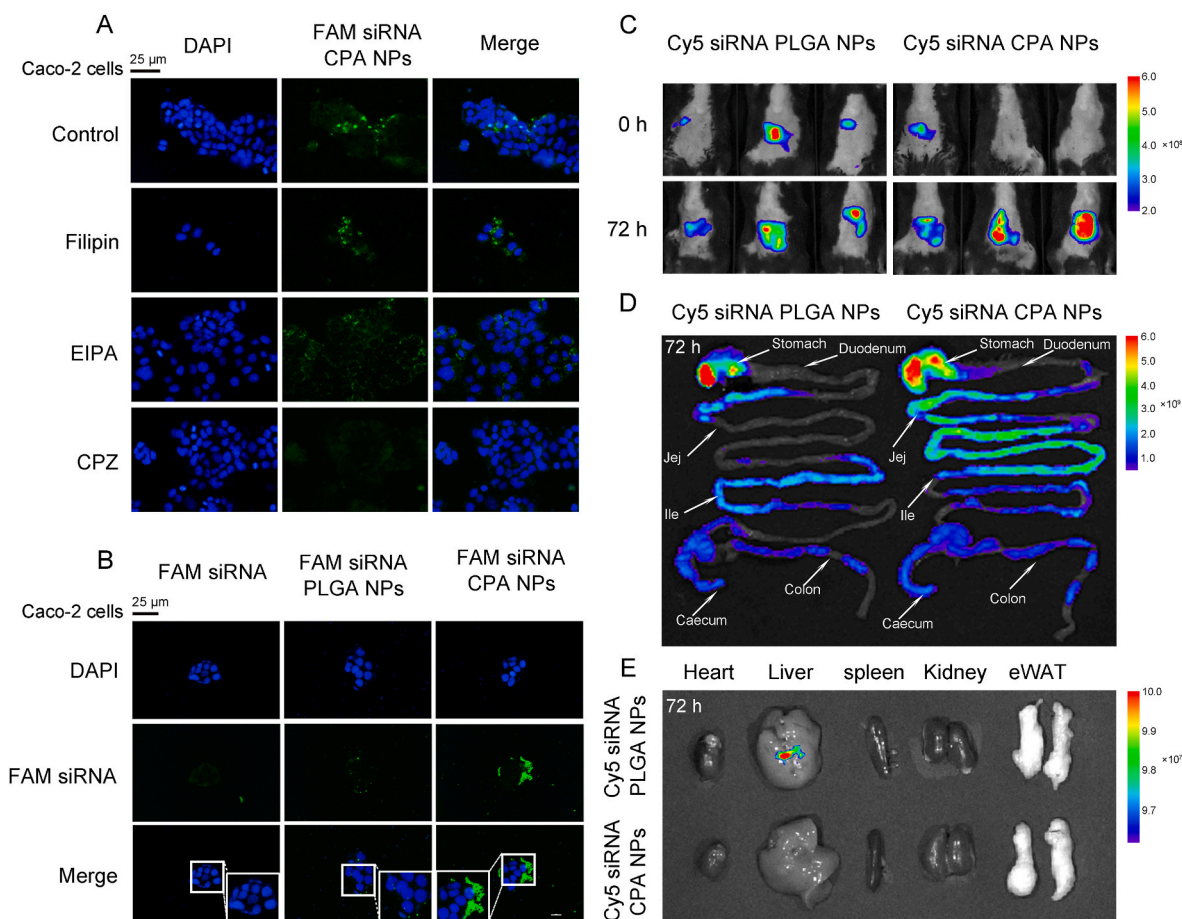


Fig. 3. Mechanism of cellular uptake and biodistribution of CPA NPs *in vitro* and *in vivo*. (A) Representative fluorescence microscopy images of Caco-2 cells treated with either FAM siRNA CPA NPs alone or in combination with indicated inhibitors (scale bars: 25 μm). (B) Fluorescence microscopy images of Caco-2 cells transfected with FAM siRNA PLGA NPs or FAM siRNA CPA NPs (scale bars: 25 μm). (C) Distribution of the indicated CPA NPs *in vivo*. (D) Representative images of the intestinal tract of mice 72 h after administration of either Cy5 siRNA PLGA NPs or Cy5 siRNA CPA NPs by intragastric administration. (E) Biodistribution of Cy5 siRNA PLGA NPs and Cy5 siRNA CPA NPs in the mouse liver, eWAT, spleen, kidney and heart. Quantitative data were presented as mean \pm SD.

3.3. Biosafety analysis of CPA NPs

To investigate the potential toxic effects of CPA NPs, we treated Caco-2 cells with different components or doses of CPA NPs. We found that none of them affected the cell viability of Caco-2 cells, indicating that CPA NPs were safe for intestinal cells (Figure S3A and S3B). More importantly, CPA NPs modestly affected the mouse body weight and food intake when compared to the PBS-treated group (Figure S3C and S3D). In addition, we did not observe any changes in serological hepatic injury parameters, including ALT and AST (Figure S3E). Similar results were observed for renal injury markers, such as serum creatinine and BUN (Figure S3F and S3G). Histologically, we found that no significant differences existed in any examined organs between groups (Figure S3H).

3.4. MMP-12-siRNA-CPA NPs improve HFD feeding-induced obesity and insulin resistance

To further identify the specific role of MMP-12 in mouse small intestines, we used a state-of-art CPA NP system carrying an MMP-12 siRNA mixture to construct mice with small intestine-specific MMP-12 knockdown (with $93.46 \pm 0.54\%$ encapsulation efficiency, Figure S4A). The CPA NPs-mediated knockdown efficiency and specificity are shown in Figure S4B-S4E. Note that enzyme-linked immunosorbent assay (ELISA) analysis revealed that knockdown of MMP-12 in mouse small intestines significantly reduced the serum and fecal levels of MMP-12, indicating that the small intestine was a dominant organ for MMP-12 secretion (Figure S4F). As shown in Fig. 4A and B, the MMP-12-siRNA-CPA NPs-treated mice had a lower ratio in body weight gain than the non-intervention mice. Meanwhile, the food intake was

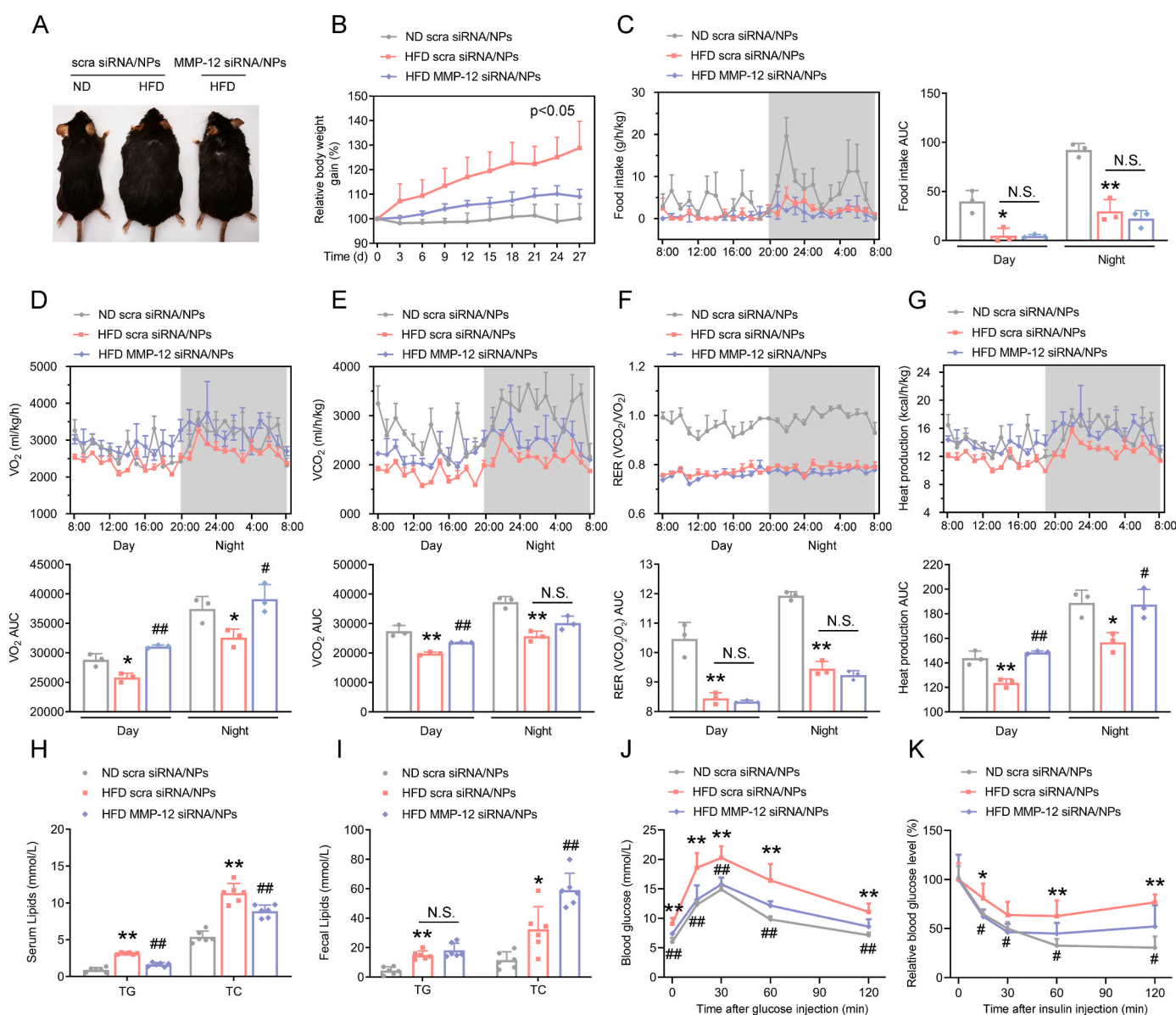


Fig. 4. MMP-12-siRNA-CPA NPs improve HFD feeding-induced obesity and insulin resistance in mice. ND and HFD mice were treated with either MMP-12-siRNA NPs or scra-siRNA NPs every 3 days for a total of 27 days through intragastric administration. (A) Representative mice were photographed at the end of the experiment. (B) Relative body weight gain, $N = 6$ for each group. (C–G) Food intake, VO_2 , VCO_2 , respiration exchange ratio (RER) (VCO_2/VO_2) and heat production were assessed by metabolic cage analysis, $N = 3$ for each group. N.S.: no significance, $*P < 0.05$, $**P < 0.01$ vs. ND scra siRNA/NPs group, $\#P < 0.05$, $\#\#P < 0.01$ vs. HFD scra siRNA/NPs group. (H and I) Serum and fecal lipid levels. (J and K) GTT and ITT analyses, $N = 6$ for each group. N.S.: no significance, $*P < 0.05$, $**P < 0.01$ vs. ND scra siRNA/NP group, $\#P < 0.05$, $\#\#P < 0.01$ vs. HFD scra siRNA/NPs group. Quantitative data were presented as mean \pm SD. Significance was established using one-way ANOVA followed Tukey's multiple comparisons test. Je: jejunum; Ile: ileum.

modestly altered by MMP-12-siRNA-CPA NPs in HFD-fed mice (Fig. 4C). Since the small intestine is an important organ for maintaining lipid homeostasis and contributes essentially to obese development, we determined the impact of MMP-12 knockdown on whole-body energy metabolism using metabolic cage analysis. We found that administration of MMP-12-siRNA-CPA NPs significantly increased O₂ consumption, CO₂ production and heat production in HFD-fed mice (Fig. 4D–G). Consistently, HFD feeding-induced hypertriglyceridemia, hypercholesterolemia, fasting hyperglycemia, hyperinsulinemia, the increased homeostasis model assessment (HOMA) of insulin resistance (HOMA-IR), and hyperlipidemia were alleviated in these mice (Fig. 4H, S4G and S4H). In contrast, the fecal levels of TC and NEFAs were correspondingly increased (Fig. 4I and S4I). In parallel, glucose intolerance and insulin sensitivity were correspondingly improved by MMP-12 knockdown (Fig. 4J and K, S4J and S4K). These results suggested that the overall metabolic disorders were attenuated by MMP-12 manipulation.

3.5. MMP-12-siRNA-CPA NPs ameliorate HFD feeding-induced hepatic steatosis, adiposity and systemic inflammation

Given that impaired insulin sensitivity facilitates the pathological progression of hepatic steatosis, adiposity and systemic inflammation [30], we next examined the effects of MMP-12-siRNA-CPA NPs on these pathological parameters in HFD-fed mice. Morphological analysis

indicated that administration of MMP-12-siRNA-CPA NPs significantly decreased the sizes of the liver and adipose tissues from HFD-fed obese mice (Fig. 5A, S5A and S5B). In parallel, histological analyses revealed that large lipid droplets were existed in sections of the liver and the WAT from HFD-fed obese mice. Such a pathological lipid accumulation was alleviated by the treatment of MMP-12-siRNA-CPA NPs (Fig. 5B, S5C and S5D). These changes of hepatic lipid accumulation were further confirmed by boron-dipyrromethene (BODIPY) staining (Fig. 5C). Notably, the liver contents of TG and TC, as well as serum levels of transaminases, were decreased in MMP-12-siRNA-CPA NPs-treated mice, when compared to the HFD-fed mice (Fig. 5D and E). At the inflammatory level, MMP-12-siRNA-CPA NPs treatment significantly decreased HFD feeding-induced macrophage infiltration in the liver, eWAT and subcutaneous white adipose tissue (sWAT), as evidenced by IF analysis of F4/80 expression (Fig. 5F). Additionally, since the adipose tissues are main sources of inflammation in obesity [36], we examined the levels of inflammatory cytokines and adipokines, including interferon-6 (IL-6), IL-1 β , tumor necrosis factor- α (TNF- α), monocyte chemoattractant protein-1 (MCP-1) and adiponectin (ADPN). As shown in Figure S5E, we found that administration of MMP-12-siRNA-CPA NPs attenuated the protein expression levels of inflammatory cytokines, while increased the anti-inflammatory adipokine ADPN expression. Consistently, serological analysis of inflammatory cytokines, including IL-6, TNF- α , and MCP-1, were decreased in these mice treated with

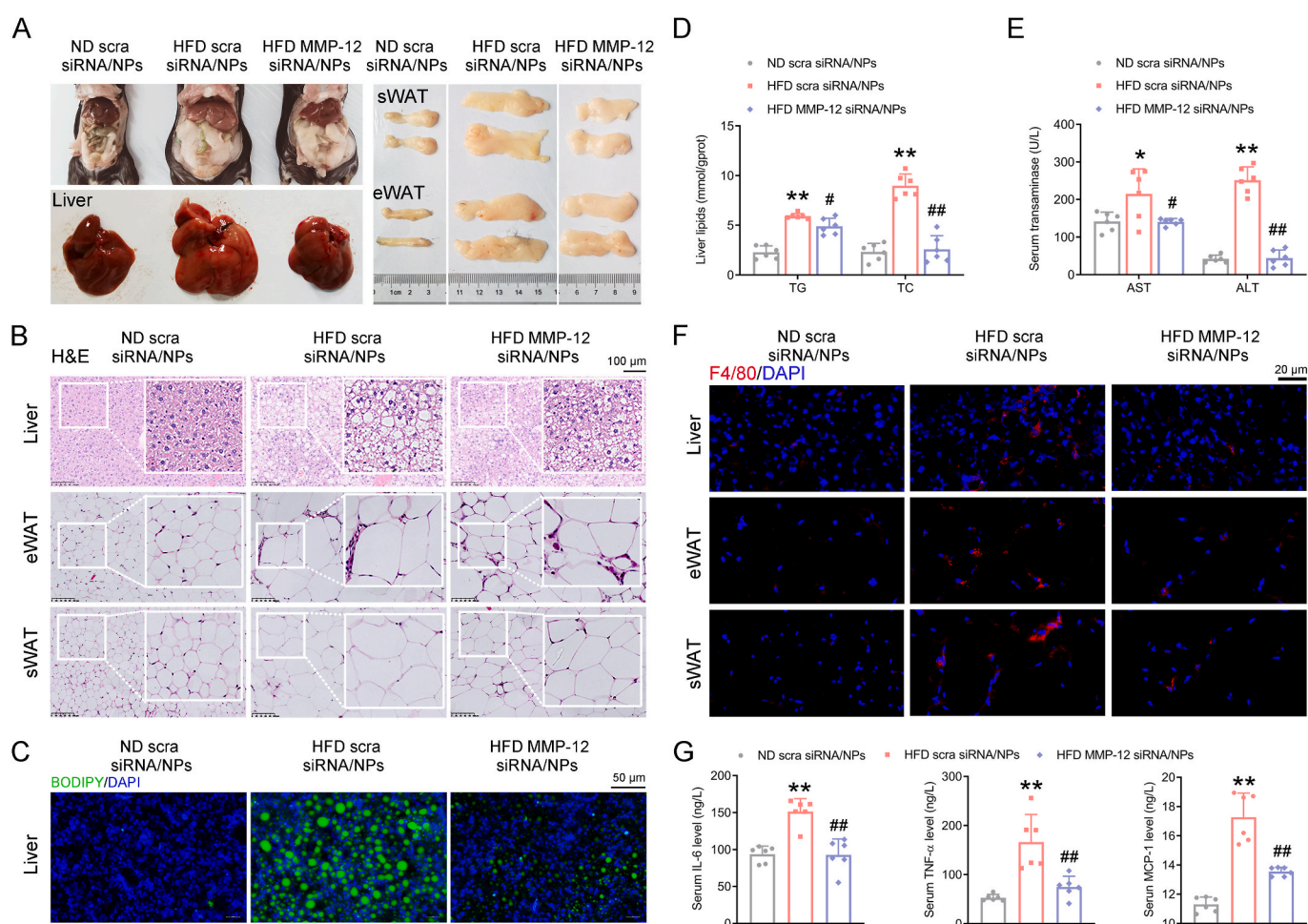


Fig. 5. MMP-12-siRNA-CPA NPs ameliorate HFD feeding-induced hepatic steatosis, adiposity and systemic inflammation. (A) Morphologic photos of humanely killed mice (left, upper); Representative images of liver (left, below), eWAT and sWAT (right). (B) Representative images of H&E staining for liver, eWAT and sWAT sections (scale bars: 100 μ m). (C) BODIPY staining for liver lipid accumulation (scale bars: 50 μ m). (D) Liver TG and TC contents. (E) Serum transaminases. (F) IF analysis of F4/80 expression in the liver, eWAT and sWAT (scale bars: 50 μ m). (G) Serum IL-6, MCP-1 and TNF- α levels. $N = 6$ for each group, * $P < 0.05$, ** $P < 0.01$ vs. ND scra siRNA/NP group, # $P < 0.05$, ## $P < 0.01$ vs. HFD scra siRNA/NPs. Quantitative data were presented as mean \pm SD. Significance was established using one-way ANOVA followed Tukey's multiple comparisons test.

MMP-12-siRNA-CPA NPs (Fig. 5G). These results confirmed that HFD feeding-induced systemic inflammation was ameliorated by MMP-12-siRNA-CPA NP treatment.

3.6. MMP-12-siRNA-CPA NPs improve lipid transportation and BA reabsorption in the small intestines of HFD-fed mice

To identify the potential mechanism underlying the protective effects of MMP-12 knockdown in the mouse small intestines on diet-induced obesity, we next performed transcriptional profiling on small intestine samples (a mixture of jejunum and ileum) to globally screen out the downstream events of MMP-12. As shown in Fig. 6A, MMP-12 knockdown increased the expression levels of 630 genes. In contrast, the expression levels of 454 genes were decreased. Gene ontology (GO) analysis revealed that a cluster of activated genes was involved in the immune responses and fatty acid metabolism, while the suppressed genes were clustered into the lipid transportation and cholesterol metabolism (Fig. 6B). Hence, we examined whether MMP-12 was essential for the transport of dietary lipid absorption into the circulation since the small intestine is an important organ for such a process. As shown in Fig. 6C, postprandial TG response assays indicated that

administration of MMP-12-siRNA-CPA NPs markedly decreased serum TG levels in HFD-fed mice. Histological and BODIPY staining analyses indicated that refeeding-induced lipid accumulation in the enterocytes of the mouse small intestines was almost absent in these mice (Fig. 6D).

Of note, chylomicron contributes importantly to mediating the transportation of dietary lipids into the circulation system [14]. TEM scanning analysis indicated that smaller chylomicron particles existed in the serum from MMP-12 knockdown mice after 2-h HFD refeeding compared to the control group (Fig. 6E, S6A and S6B). Coincident with these findings, the serum collected from 2-h HFD-refed mice administered MMP-12-siRNA-CPA NPs was transparent, whereas the control serum was milky (Fig. 6E). At the molecular level, ApoB-48 contents in the chylomicron fraction and serum were correspondingly reduced, while its expression was consistently reduced in mouse small intestines (Fig. 6F and S6C).

BAs are involved in the absorption and metabolism of dietary lipids in the small intestines, as well as gut permeability and bacterial composition [21]. As shown in Fig. 6G, we found that serum levels of total BAs were decreased by approximately 45.15% in HFD-fed mice treated with MMP-12-siRNA-CPA NPs compared to HFD-fed mice. Furthermore, we examined the mRNA expression levels of BA

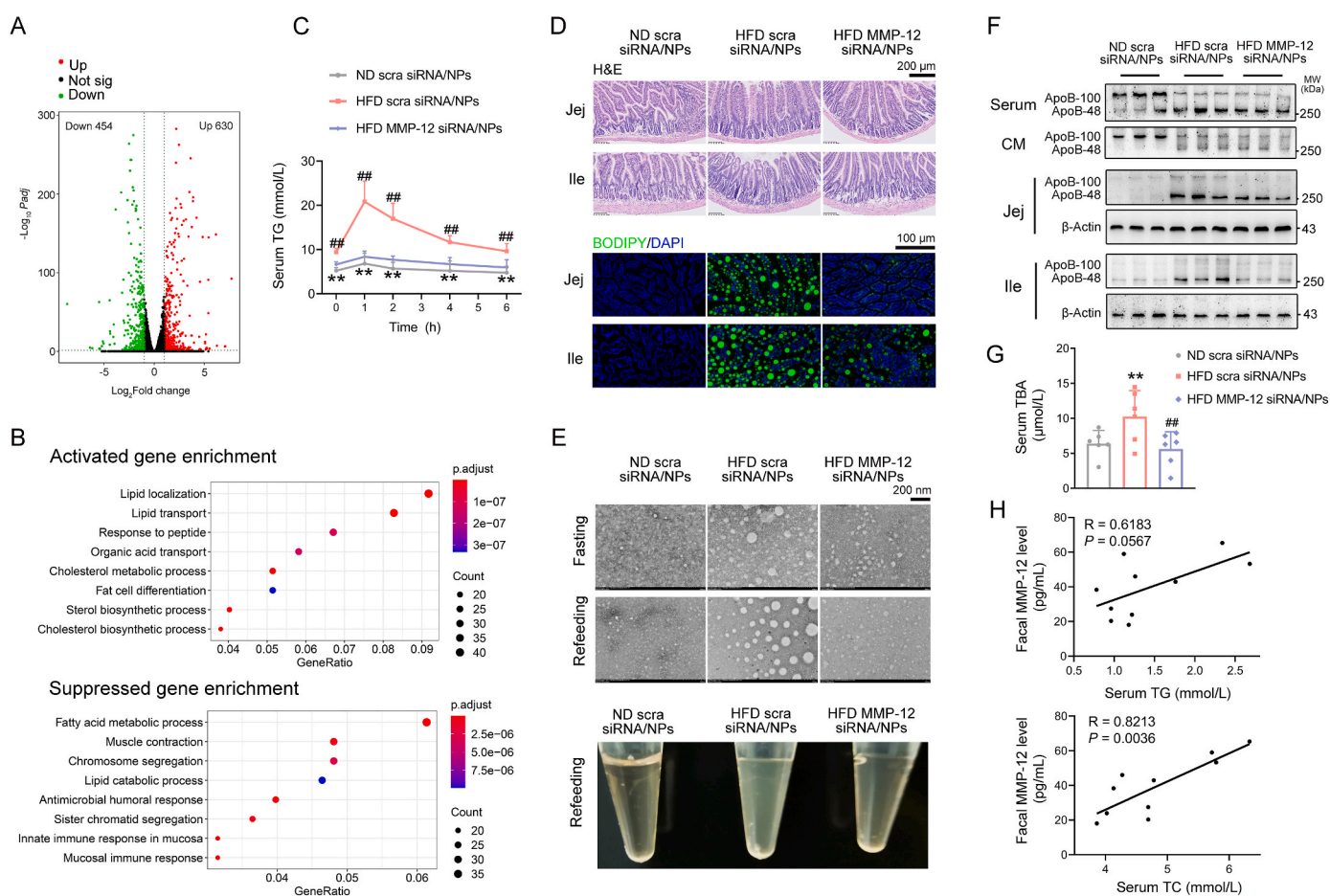


Fig. 6. MMP-12-siRNA-CPA NPs improve lipid transportation and BA reabsorption in the small intestines of HFD-fed mice. (A) Genome-wide changes in mRNA expression shown in a volcano plot. The number of genes up- or downregulated by 2-fold or more with $P < 0.05$. (B) GO analysis of biological pathways using the ClusterProfiler package of R software. (C) Postprandial TG response in mice after oral gavage with olive oil (10 $\mu\text{L}/\text{body weight}$), $N = 6$ for each group. $**P < 0.01$ vs. ND scra siRNA/NP group, $###P < 0.01$ vs. HFD scra siRNA/NPs. (D) H&E (scale bars: 200 μm) and BODIPY (scale bars: 100 μm) staining of intestine sections from three different groups of mice after oral gavage with olive oil for 2 h. (E) Serum chylomicron particle size in mice (upper) and a representative picture of serum collected from mice (below) (scale bars: 200 nm). (F) Western blot analysis of ApoB-48 expression in mouse serum, chylomicron, jejunum and ileum. (G) Serum total BA (TBA) levels. For A-G, $N = 6$ for each group. $**P < 0.01$ vs. ND scra siRNA/NP group, $###P < 0.01$ vs. HFD scra siRNA/NPs. Quantitative data were presented as mean \pm SD. Significance was established using one-way ANOVA followed Tukey's multiple comparisons test. (H) Correlation of serum TG and TC levels with fecal MMP-12 levels in human subjects, $N = 10$ for each group. The correlation coefficients (R value) and P values were calculated by Pearson analysis. CM: chylomicron; Jej: jejunum; Ile: ileum.

reabsorption biomarkers in the mouse jejunum and ileum, including *Asbt*, *Ibabp*, *Osta* and *Ostb*, and found that they were downregulated in response to MMP-12 knockdown (Figure S6D), which is consistent with the reduced serum levels of BAs in these mice. Furthermore, fecal levels of MMP-12 and serum lipids were positively correlated in clinical samples (Fig. 6H).

3.7. MMP-12-siRNA-CPA NPs attenuate inflammation and maintain the permeability of mouse small intestines

We next explored the inflammatory status in the small intestines of HFD-fed mice treated with MMP-12-siRNA-CPA NPs. As shown in Fig. 7A, HFD feeding significantly decreased the small intestine length, which was reversed by MMP-12 knockdown. Histological analysis indicated that MMP-12-siRNA-CPA NPs significantly attenuated HFD feeding-induced villous atrophy and crypt hyperplasia (Fig. 7B). Since intestinal goblet cells contribute importantly to intestinal mucin

excretion, we therefore examined the numbers of these cells using alcian blue and periodic acid Schiff (AB-PAS) staining. As shown in Fig. 7B, HFD feeding decreased the numbers of goblet cells in the mouse small intestines compared to the normal diet (ND) feeding groups. MMP-12-siRNA-CPA NPs treatment restored this reduction. To confirm the severity of intestinal inflammation, we evaluated macrophage (F4/80-positive), neutrophil (Gr-1-positive), and T lymphocyte (CD4-positive) infiltration. Compared with modest changes observed in the ND group, HFD-fed mice displayed increased immune cell infiltration in the small intestines. In contrast, administration of MMP-12-siRNA-CPA NPs dramatically blocked these infiltrations (Fig. 7C). Accordingly, the mRNA expression levels of pro-inflammatory cytokines, including *Il-1β* and *Tnf-α*, were markedly reduced in the small intestines of these mice (Figure S7A). These results indicated that MMP-12 was a critical mediator in HFD feeding-induced small intestinal inflammation.

Small intestinal permeability is affected by inflammation under metabolic stress [37]. We found that HFD feeding induced marked tight

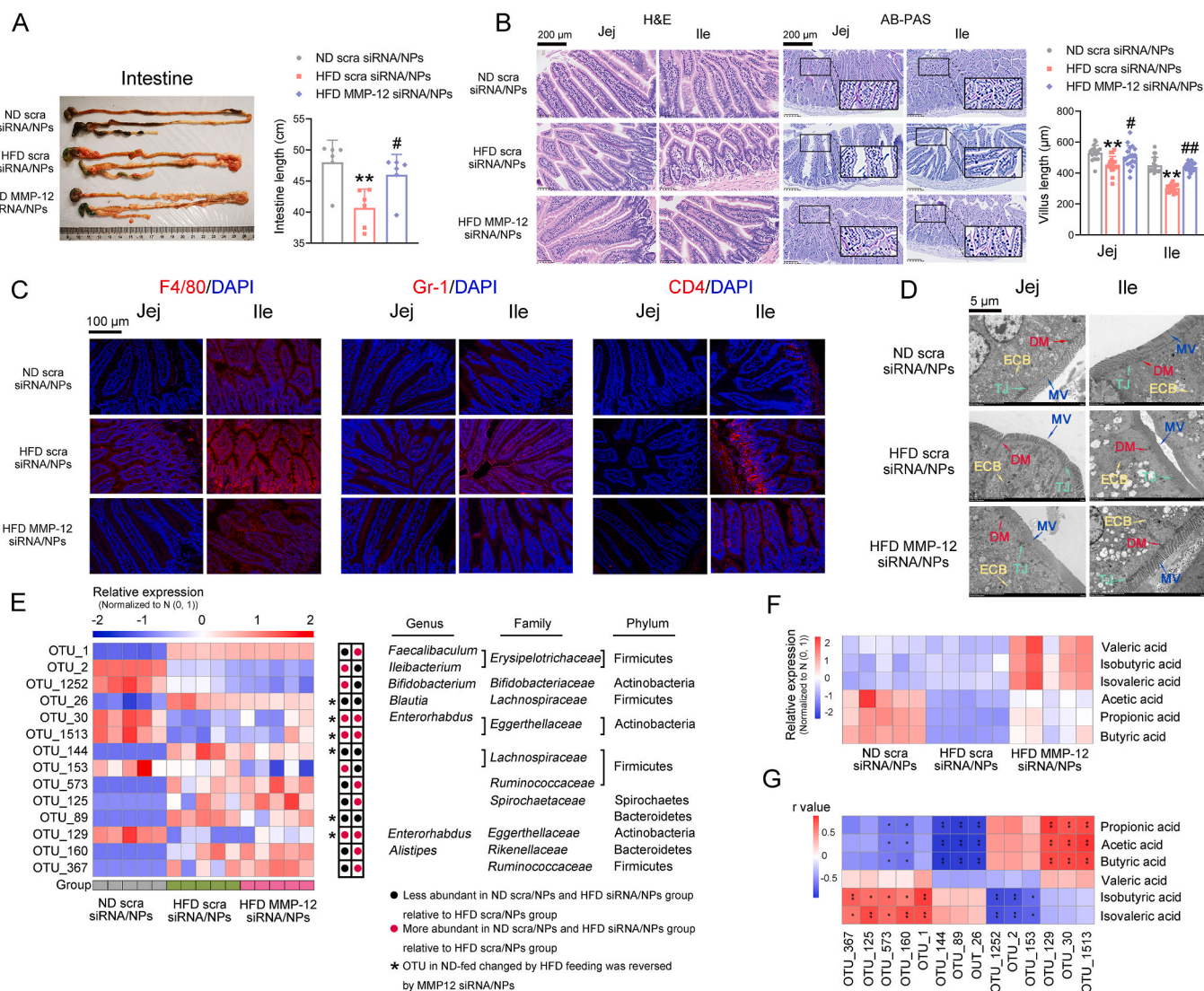


Fig. 7. MMP-12-siRNA-CPA NPs attenuate inflammation and maintain the permeability of mouse small intestines. (A) Typical shape (left) and length (right) of the small intestines. (B) H&E and AB-PAS staining of small intestines (scale bars: 200 μm). (C) F4/80, Gr-1 and CD4 expression in the small intestines was assessed by IF staining (scale bars: 100 μm). (D) TEM analysis of jejunum (left) and ileum (right) epithelial cells. Key morphological features, such as the microvilli (MV), TJ, epithelial cell border (ECB), and desmosome (DM), are indicated (scale bars: 5 μm). For A-D, N = 6 for each group. **P < 0.01 vs. ND scra siRNA/NP group, #P < 0.05, ##P < 0.01 vs. HFD scra siRNA/NPs. Quantitative data were presented as mean ± SD. Significance was established using one-way ANOVA followed Tukey's multiple comparisons test. (E) Abundance heatmap of 14 OTUs significantly changed by MMP-12 siRNA/NPs in HFD-fed mice based on RDA, N = 5 for each group. (F) Abundance heatmap of significantly changed SCFAs, N = 5 for each group. (G) Heatmap of Spearman correlation analysis between changed OTUs and SCFAs. *P < 0.05, **P < 0.01. Jej: jejunum; Ile: ileum.

junction (TJ) impairments in the mouse small intestinal epithelium, as evidenced by increased serum levels of D-Lac, impaired TJ structure and reduced protein expression levels of TJ biomarkers, including Occludin and ZO-1. In contrast, MMP-12-siRNA-CPA NPs intervention significantly attenuated these impairments by restoring them close to the levels of the ND-fed group (Fig. 7D, S7B–S7D). Of note, the beneficial effects of MMP-12-siRNA-CPA NPs were further confirmed by *in vitro* studies with increased levels of TJ-associated protein expression and transepithelial electrical resistance (TEER) (Figure S8A–S8C). Therefore, we speculate that FFAs may influence intestinal permeability through the regulation of MMP-12. These results suggested that MMP-12 was a critical factor in mediating the HFD feeding-induced permeability impairments of mouse small intestines.

3.8. MMP-12-siRNA-CPA NPs alter the composition of gut microbiota and SCFAs

Gut dysbiosis has been shown to facilitate the development of obesity, whereas obesity further disrupts the composition of gut microbiota, thus forming a vicious circle [18]. By using bacterial 16 S rRNA sequencing (V4 region), a total of 1,648,417 raw reads were obtained after qualification and were annotated to 699 OTUs. Rarefaction analysis showed that the current sequencing depth covered almost all the gut microbiota within each sample (Figure S9A and S9B). Unsupervised principal coordinate analysis (PCoA) was used to analyze the whole structural alterations in the gut microbiota among groups. Along the PCo2 axis, MMP-12-siRNA-CPA NPs treatment reversed HFD feeding-induced dysbiosis, whereas no significant changes were observed in the structure along PCo1 (Figure S9C). Unweighted pair-group method with arithmetic mean (UPGMA) analysis indicated significant separations in the microbiota between ND- and HFD-fed mice and between HFD-fed groups in presence with or without MMP-12-siRNA-CPA NPs, suggesting that MMP-12 knockdown could alter the microbiota composition and shift the microbial community profile from a HFD feeding-induced dysbiotic state towards homeostasis in ND-fed mice (Figure S9D). In addition, taxonomic profiling revealed that MMP-12-siRNA-CPA NPs administration markedly reduced the contents of the *Proteobacteria* phylum in the feces from HFD-fed obese mice (Figure S9E–S9H). Given that the *Proteobacteria* phylum is a well-known infective pathogen that contributes to the development of metabolic endotoxemia, MMP-12-siRNA-CPA NPs consistently reduced serum levels of LPS in HFD-fed mice (Figure S9I). Such a reduction in LPS could be a critical explanation for the alleviated inflammation in these mice.

Next, we used redundancy analysis (RDA) to clarify the specific bacterial phylotypes changed by HFD signals and MMP-12-siRNA-CPA NPs treatment (Figure S9J). Compared to the ND-fed group, HFD signals dramatically altered the 228 OTUs, among which 167 were upregulated and 61 were downregulated. In HFD-fed mice, administration of MMP-12-siRNA-CPA NPs altered 14 OTUs (8 upregulated and 6 downregulated). Interestingly, 6 OTUs were altered by both HFD feeding and MMP-12-siRNA-CPA NPs administration, and their changes exhibited opposite trends. Among these, OTU_26 and OTU_144 were classified in the detrimental *Lachnospiraceae* family. This family belongs to the *Firmicutes* phylum, which is known to aggravate LPS transfer into the circulation system. In addition, 3 OTUs (OTU_30, OTU_1513 and OTU_129) were annotated to the beneficial *Eggerthellaceae* family, which is a beneficial bacterium responsible for metabolizing secondary plant polyphenols to ameliorate gut inflammation (Fig. 7E and Table S4).

Among gut microbiota-generated metabolites, SCFAs, which are metabolized by intestinal microbiota through indigestible carbohydrates, have been determined to downregulate inflammatory cytokine production in macrophages. We thus evaluated the contents of 6 dominant SCFAs in mouse feces. As shown in Fig. 7F and Table S5, HFD signals significantly reduced the contents of SCFAs compared to ND signals. In contrast, such a reduction was reversed by MMP-12-siRNA-

CPA NPs treatment. Coincident with these results, Spearman correlation analysis revealed that MMP-12-siRNA-CPA NPs-induced substantial elevation of SCFAs, including propionic acid, acetic acid and butyric acid, was positively correlated with 3 beneficial OTUs (OTU_30, OTU_1513 and OTU_129) but negatively correlated with 2 detrimental OTUs (OTU_26 and OTU_144) (Fig. 7G, Table S6 and S7), suggesting that these OTUs are essential bacteria in MMP-12 knockdown-regulated SCFA production.

Taken together, these data suggested that MMP-12-siRNA-CPA NPs may exert their anti-inflammatory effects and improve gut health by regulation of the gut bacterial composition and the production of the SCFAs.

3.9. GM6001-CPA NPs modestly affect HFD feeding-induced obesity

To further dissect whether these beneficial roles of MMP-12 knockdown in mouse small intestines were dependent on its reduced enzymatic activity or expression, we used the CPA NPs system carrying the pan-MMP inhibitor GM6001 (100 mg/kg, GM6001/CPA NPs diameter: 209.4 nm; Encapsulation efficiency: $91.73 \pm 1.74\%$, Figure S10A) to neutralize all the MMP enzymatic activity, in case of the compensatory effects from other MMPs. As shown in Figure S10B, GM6001 significantly decreased the enzymatic activity of MMP-12 in the small intestines of mice fed a HFD. However, GM6001-CPA NPs modestly affected the HFD feeding-induced increase in body weight gain as well as the reduction in food intake (Figure S10C and S10D). In addition, HFD feeding increased blood glucose levels and impaired glucose tolerance, while GM6001-CPA NPs did not alter these parameters. Morphologically, administration of GM6001-CPA NPs modestly affected HFD feeding-induced fasting hyperglycemia, hyperlipidemia, hypercholesterolemia, and glucose intolerance (Figure S10E–S10G). Similarly, HFD feeding-induced hepatic and epididymal fat accumulation was unaltered in GM6001-CPA NPs-treated obese mice (Figure S10H–S10K). In addition, HFD signals, including increased serum AST and ALT, as well as TG and TC, were similarly unchanged (Figure S10L and S10M). Consistently, administration of GM6001-CPA NPs modestly affected the size of adipose tissue and lipid droplets in the mouse liver (Figure S10N and S10O). In addition, the inflammatory cytokines, such as IL-6 and MCP-1, were decreased in response to GM6001 treatment at both the serological and protein expression levels, while protein expression levels of IL-1 β , TNF- α and ADPN were modestly affected by GM6001 (Figure S11A and S11B). The systemic reduction of IL-6 and MCP-1 levels may due to the possibility of unavoidable free PLGA NPs, which may carry minor doses of GM6001 and circulate in blood after passing enterocytes, further delivering GM6001 into various tissues. Given the known K_i value of GM6001 is 3.6 nM on the enzymatic activities of all MMPs [38], the potential minor doses of GM6001 in circulation system may also cause a minor improvement of systemic inflammation. Taken together, these data revealed that the beneficial role of MMP-12 knockdown was not dependent on its enzymatic function.

3.10. *Fabp4* serves as an effector of MMP-12 in the small intestines of HFD-fed mice

It should be noted that MMP-12 exerts DNA-binding abilities to control gene expression in the nucleus [39]. As shown in Fig. 8A, we found that HFD feeding significantly increased the nuclear and cytosolic contents of MMP-12 proteins in mouse small intestines (jejunum and ileum). Similar results were observed in the *in vitro* analysis (Fig. 8B). Considering the modest effect of the MMP-12 inhibitor, we speculated that MMP-12 indeed functions as a transcriptional factor involved in the regulation of small intestinal homeostasis. Hence, we performed Spearman correlation analysis to evaluate potential associations among intestinal gene expression, gut microbiota composition and SCFA contents. Venn analysis clustered 2 genes, including *Fabp4* and *Nnmt*, which were positive, in line with the above beneficial effects of MMP-12

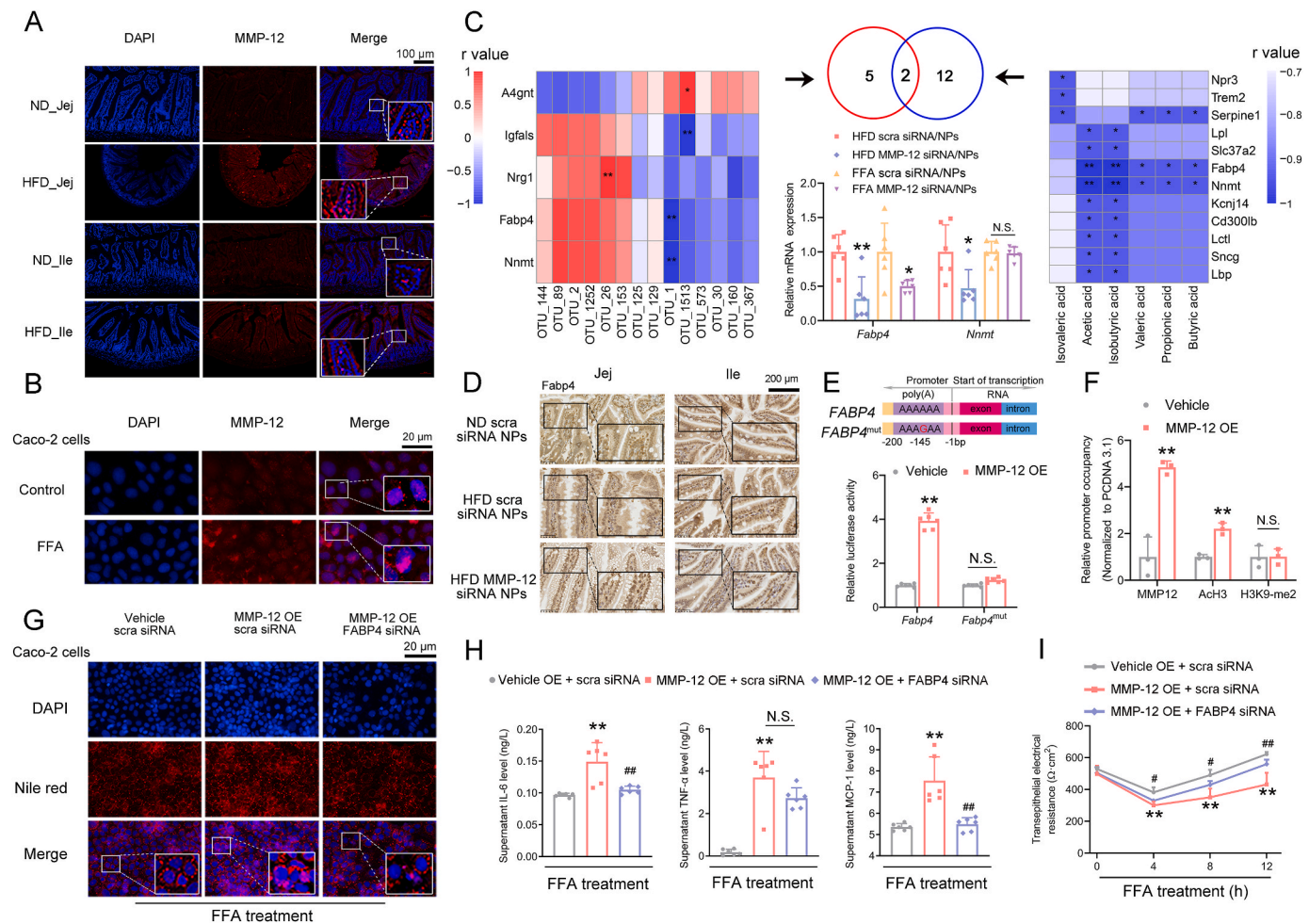


Fig. 8. *Fabp4* serves as an effector of MMP-12 in the small intestines of HFD-fed mice. (A and B) IF analysis of cytosolic and nuclear MMP-12 protein expression in mouse small intestines (jejunum and ileum) (scale bars: 100 μ m) and Caco-2 cells (scale bars: 20 μ m). (C) Heatmap of Spearman correlation analysis between changed small intestinal gene expression and OTUs (left), * P < 0.05, ** P < 0.01. Heatmap of Spearman correlation analysis between changed small intestinal gene expression and SCFA contents (right), * P < 0.05, ** P < 0.01. Venn diagrams and RT-qPCR validation of correlation analyses (middle), * P < 0.05, ** P < 0.01 vs. HFD scra siRNA/NPs or FFA scra siRNA/NPs group. (D) IHC analysis of *Fabp4* expression (scale bars: 200 μ m). (E) Luciferase activity of the *FABP4* promoter or *FABP4*^{mut} promoter in Caco-2 cells transfected with vehicle or MMP-12 plasmids, N = 6 for each group. (F) ChIP assays with the indicated antibodies in Caco-2 cells transfected with vehicle or MMP-12 plasmid, N = 3 for each group. ** P < 0.01 vs. vehicle group. Caco-2 cells were transfected with the indicated plasmid or siRNA for 24 h and then treated with 0.4 mM FFAs for another 24 h. (G) Nile red staining (scale bars: 20 μ m). (H) Supernatant IL-6, MCP-1 and TNF- α levels. (I) The TEER levels, N = 5 for each group. * P < 0.05, ** P < 0.01 vs. Vehicle + scra siRNA group, # P < 0.05, ## P < 0.01 vs. MMP-12 overexpression (OE) + *FABP4* siRNA group. Quantitative data were presented as mean \pm SD. Significance was established using one-way ANOVA followed Tukey's multiple comparisons test. Jej: jejunum; Ile: ileum. (For interpretation of the references to color in this figure legend, the reader is referred to the Web version of this article.)

knockdown (Fig. 8C and Table S8-S11). We further evaluated the mRNA expression levels of these two genes in response to MMP-12 knockdown *in vivo* and *in vitro* and found that *Fabp4* mRNA expression was most robustly decreased in the small intestines of HFD-fed mice treated with MMP-12 siRNA NPs and in FFA-treated Caco-2 cells with MMP-12 knockdown (Fig. 8C). The protein expression of *FABP4* exhibited a similar tendency (Fig. 8D and S12A-S12D).

Bioinformatics analysis indicated that a classic MMP-12-binding motif featuring a poly(A) tract of 6 bases was present on the proximal promoter of *FABP4* (−148 bp — −142 bp, Fig. 8E). Luciferase activity analysis indicated that overexpression of MMP-12 significantly increased the transcriptional activity of the *FABP4* promoter. However, such an activation effect was abolished when this poly(A) tract was mutated (Fig. 8E). Consequently, the mRNA and protein expression levels of *FABP4* were correspondingly increased in MMP-12-overexpressing Caco-2 cells (Figure S12E and S12F). At the epigenetic level, acetyl-histone H3 (ACh3) and K9-dimethylated histone H3 (H3K9-me2) are two hallmarks associated with chromatin activity and gene transcription [33]. In our study, overexpression of MMP-12 led to robust ACh3

(activation) accumulation, accompanied by a modest impact on the H3K9-me2 levels around the *FABP4* proximal promoter (Fig. 8F), suggesting that MMP-12 is a potential enhancer of *FABP4* transcription by increasing the accumulation of histone acetylation. Next, we wanted to explore whether *FABP4* linked MMP-12 signals to the homeostasis of the small intestinal homeostasis. We knocked down *FABP4* expression in MMP-12-overexpressing Caco-2 cells. The knockdown efficiency of *FABP4* siRNA and the overexpression efficiency of MMP-12 are presented in Figure S10G. We found that knockdown of *FABP4* partially antagonized MMP-12-facilitated lipid accumulation, pro-inflammatory cytokine expression and secretion, and TJ impairment (Fig. 8G–I and S12G).

In addition, we examined the protein expression levels of other *Fabps*, including *Fabp1/2/3/5/6/7/12*, that were expressed in mouse small intestines [40]. As shown in Figure S13, HFD feeding increased *Fabp1/2/5/6/12* protein expression levels, while decreased the *Fabp7* in mouse small intestines. Given the increased *Fabp4* levels, these data collectively indicated that the small intestinal *Fabp* family plays potential roles in correspondence to HFD feeding signals. Meanwhile, we

noticed that protein expression levels of Fabp1/5/7 were further increased, when MMP-12 was knocked down. Such an increase of these Fabp proteins may be caused by an unexpected compensatory effect, which has been documented by other studies [41,42]. In our study, the endogenous expression levels of Fabp1/5/7 are less than that of Fabp4 in the small intestine of HFD-fed mice (Figure S12A and S13). Hence, these undesired increases may fail to antagonize the net beneficial effect of MMP-12 knockdown-decreased Fabp4 expression.

4. Discussion

MMP-12 is a macrophage metal elastase that cleaves elastin, which is a major component in the media of the small intestines. Macrophages are the major source of MMP-12, the expression of which is markedly increased in various inflammatory diseases [25,43]. Given the causative relationship between inflammation and obesity, MMP-12 expression is increased in mouse WAT in response to HFD-feeding signals. Although MMP-12 is also expressed in the small intestines, whether it contributes to homeostasis and whole-body metabolism remains elusive. In the present study, our findings revealed that HFD signals induced marked MMP-12 expression in mouse small intestines and feces. To specifically and effectively knock down MMP-12 in the small intestines of HFD-fed mice, we successfully constructed an NP system to effectively and orally deliver MMP-12 siRNA. Making the best of this NPs system, we found that small intestine-specific MMP-12 knockdown improved HFD feeding-induced metabolic disorders, including hyperglycemia, hyperinsulinemia, glucose intolerance, impaired insulin sensitivity and systemic inflammation. In addition, the HFD-feeding-induced disruptions of lipid uptake/transportation, BA reabsorption, permeability and inflammation in mouse small intestines were recuperated by MMP-12 knockdown. We also revealed that small intestinal MMP-12 exerts DNA-binding abilities in the cellular nucleus, rather than its elastolytic activity, when corresponding to HFD-feeding signals, while FABP4 served as its key transcriptional downstream effector. Our findings shed some light on the pathophysiological and transcription-regulatory function of MMP-12 and developed a state-of-the-art siRNA delivery system for gene-specific intervention in mouse small intestines.

To tissue-specifically regulate MMP-12 expression, we first focused on small intestines and designed a CPA NPs system. Given the extensive applications of nanotechnology in delivering various RNAs into tumors [44–46], herein, we developed a novel NPs system for the systemic delivery of siRNA into the small intestines to treat metabolic diseases. Our findings broadened the current applications of the NPs system for gene therapies for metabolic disorders. In our present study, CPA NPs exert the following beneficial advantages. For basal materials, CS, isolated from lobsters, crabs and other marine invertebrates, is safe and biocompatible, accompanied by pH-sensitive and adhesive properties [47]. Herein, we established a CS to serve as a protective shelter to avoid gastric acid and to retain the functional siRNA in the small intestines. In addition, as another core component of our NPs, PLGA is a widely used polymer with biodegradable and biocompatible abilities that has been approved in the clinic to deliver antitumor drugs for multiple cancer treatments, including colorectal cancer and ovarian cancer [35,48]. Of note, sialic acid is widely distributed and is presented with negative charge in mucins, which should prevent the negative-charged PLGA NPs penetrate through a mucus layer to small intestinal cells [49]. To overcome this problem, we coated the surface of PLGA NPs with a layer of CS and finally prepared a typical core-shell CPA NPs. Because the CS owns positive surface charge and is known to safely interact with intestinal mucosal proteins [50], CPA NPs could be effectively absorbed by small intestinal cells. We used this material as a core to coat the PLL-modified siRNAs [29]. By taking advantage of double-emulsion and ionic gelation strategies, we constructed an NPs system and effectively applied it for the *in vivo* knockdown of MMP-12 in mouse small intestines based on the protective effects of CS. Our CPA NPs system did not affect MMP-12 expression in other organs, including the liver,

kidney and colon, demonstrating its excellent specificity in the small intestines. Therefore, the CPA NPs system possesses great potential in delivering either RNAs or drugs into the small intestines. Notably, adeno-associated viruses (AAVs) have also been developed to manipulate gene expression in small intestines [51]. However, technical limitations, such as difficulties in the achievement of high-titer AAVs, still restrict the clinical applications of this method [52]. In contrast, our CPA NPs system was host-friendly due to its transient impacts on gene expression, since they were prone to be excreted by intestinal peristalsis within the feces. In addition, although MMP inhibition holds significant therapeutic potentials for the treatment of inflammatory diseases, this approach unfortunately has been hindered by significant side effects of MMP inhibitors due to the important physiologic role of MMPs in tissue remodeling. In the present study, we took advantages of the nanosystem to specifically knock down MMP-12 expression in the mouse small intestine and improve the HFD feeding-induced metabolic disorders. This strategy may partially avoid the global side effects caused by MMP inhibitors. Lastly, it does not escape our attention that the small intestines consist of various types of cells, including intestinal villous epithelial cells, columnar cells and goblet cells [53]. Moreover, when the mice were fed a HFD, neutrophils and macrophages also infiltrated into the small intestines to trigger inflammatory responses, which facilitated metabolic disorders [54,55]. In our study, we found that HFD feeding increased the accumulation of MMP-12 within the intestinal epithelial cells by using immunofluorescent analysis with cell-specific biomarkers, indicating that the ALP-positive epithelial cells were the *bona fide* venue for MMP-12's pathophysiological function. Hence, deep single-cell RNA-seq analyses and cell type-specific NPs systems based on targeted peptides should be considered for the precision treatment of MMP-12-based metabolic diseases [56–58].

Global MMP-12 deficiency mice have been generated for nearly a decade to identify the pathophysiological functions of MMP-12 [59]. However, we noticed that global MMP-12 deficiency increased the body weight, which differs from our results [60]. This discrepancy may be caused by the difference within the microenvironment of the global knockout and tissue-specific knockdown mice. This phenomenon has also been achieved in many other studies. For example, Bmal1 functions as a core clock component to orchestrate the circadian homeostasis [61]. As reported, global Bmal1 KO impairs glucose tolerance in mice [61]. In contrast, liver-specific Bmal1 deficiency improves mouse glucose tolerance [62]. Therefore, the physiological function of MMP-12 are organ-specific and based on its *bona fide* organ properties. Meanwhile, developing a tissue-specific manipulation strategy (e.g. nanosystem) targeting MMP-12 should be taken into consideration for the future clinical applications and translational medicine. On the other hand, we did not observe such a significant reduction in the body weight of HFD-fed obese mice. The potential reasons are as follows: 1. Because we only intervened with MMP-12-siRNA-CPA NPs for 27 days, we hypothesized that an extended intervention would result in a more significant decrease in obesity as determined by body weight. 2. The plausible side effects caused by the undesired increases of Fabp1/5/7 protein may partially contribute to the maintenance of the body weight in the HFD-fed mice administrated with MMP-12 siRNA CPA NPs.

In our study, the functional phenotype of MMP-12 knockdown is extensive in the alleviation of small intestinal disorders and metabolic dysfunction of HFD-fed obese mice. The possible reasons for such extensive functions of MMP-12 were as follows: 1. CPA NPs could functionally deliver the siRNA into various cells existed in the small intestines, and thus decreasing the MMP-12 expression. Hence, the beneficial effects of MMP-12 knockdown were a net cluster of all the MMP-12-expressing cells in small intestines. 2. Fabp4, as one of the potential downstream effectors of MMP-12, was also highly expressed both in paneth cells and capillary endothelium of the small intestine, while paneth cells is a critical cell type contributing to the Fabp4's secretion into the circulation system [63]. Given that secreted Fabp4 could functionally affect multiple biological processes in the liver and

adipose tissues [40], the reduction of Fabp4 induced by MMP-12 knockdown may be a possible explanation for the MMP-12's versatile functions in regulating lipid metabolism and inflammation. 3. MMP-12 is also defined as a secreted protein [64]. Consistently, we found that it was also existed in the feces of both HFD-fed obese mice and hyperlipidemic patients, indicating the underlying relationships between MMP-12 and gut microbiota. At the meanwhile, small intestine-specific MMP-12 knockdown affected the abundance of 13 OTUs and decreased the levels of *Proteobacteria* phylum independent of Fabp4, indicating such a crosstalk may contribute to the shift of bacterial composition in HFD-fed mice. Because the disrupted gut microbiota composition is a well-known determinant in the pathogenesis of metabolic disorders, while the correction of the HFD feeding-induced gut dysbiosis has been proven to treat the obesity [65], the bacterial composition could be another mediator that relaying the MMP-12's signals under HFD feeding status.

Fabps have been proved to affect lipid fluxes, metabolism and signaling within cells through facilitating the transportation of lipids to specific cellular compartments, including the mitochondrion, peroxisome, endoplasmic reticulum and nucleus [41]. In our present study, we found that the expression levels of Fabp4 were upregulated both in the small intestine of HFD-fed mice and FFA-treated Caco-2 cells in an MMP-12 dependent manner. However, Fabps are well known to play important roles in a tissue-specific manner [66]. Hence, we examined protein expression levels of other Fabps in response to MMP-12 knockdown, further confirming that Fabp4 was a potential effector of MMP-12 in the small intestine of HFD-fed obese mice. Fabp4 is abundantly expressed in the adipose tissue and macrophage, and has been documented to have a significant role in many aspects of metabolic syndrome, including dyslipidemia [40]. For example, Fabp4 deficiency can affect adipocyte biology and fatty acid metabolism to alleviate the systemic insulin resistance, dyslipidemia, and lipotoxicity associated with genetic or diet-induced obesity [67]. More importantly, Fabp4 protein is also expressed in the paneth cells and capillary endothelium of the small intestine, but not in lymph vessel [68]. In our study, the expression of Fabp4 in the small intestines was negative correlated with five SCFAs, and knockdown of Fabp4 partially attenuated MMP-12-facilitated lipid accumulation and TJ impairment in FFA-treated Caco-2 cells, further confirming the regulatory function of Fabp4 in triglyceride absorption and lipid metabolism. On the other hand, Fabp4 is also involved in the development of inflammation. For instance, a Fabp4 inhibitor can reduce saturated fatty acid-induced inflammation and ameliorate lipid deposits in the skeletal muscle, while the Fabp4-deficient macrophage exhibits a decreased ability to produce inflammatory cytokines and accumulate cholesterol esters [67]. Consistent with these findings, we found that knockdown of FABP4 partially attenuated MMP-12-facilitated pro-inflammatory cytokine expression and secretion in Caco-2 cells, indicating that Fabp4 functions as an important mediator of inflammatory signals in the small intestine. These data collectively indicated that Fabp4 is extensively involved in the regulation of triglyceride absorption and inflammatory responses in the small intestines.

Fabp4 was demonstrated as a potential downstream effector of MMP-12, it might function as a more specific and safer therapeutic target instead of MMP-12 and minimize the MMP-12 inactivity-induced side effects in future studies. However, it should be noted that Fabp4 was screened by Spearman correlation analyses based on MMP-12-orchestrated the transcriptional network, gut microbiota composition and SCFA contents, since we wanted to find out the most positive responder that was in line with the above beneficial effects of MMP-12 knockdown. By using *in vitro* analyses, we confirmed that Fabp4 was a potential downstream effector involved in the MMP-12-regulated lipid absorption, TJ permeability and inflammation. Besides, although the potential relationships between the transcriptional network and gut microbiota composition existed, the correlations were not strong enough to cover all the different expressed genes and bacterial phylum, as well

as specific OTUs. In our study, Fabp4 only exhibited a negative correlation with a specific OTU (OTU_1), which is a probiotic bacterium involved in the regulation of lactic acid formation to produce SCFAs [69]. However, 16 S rRNA sequencing revealed that MMP-12 affected the abundance of at least 14 OTUs and the *Proteobacteria* phylum. Hence, MMP-12 knockdown also corrected gut dysbiosis. Taken together, we thus believed that knockdown of MMP-12 may exert a more broad effect on the small intestinal microenvironments and metabolic dysfunction, when compared to the Fabp4 knockdown.

Considering that MMP-12 is classically identified as an elastase, we blocked MMP-12 enzymatic activity by using the MMP-specific inhibitor GM6001 [70,71]. We unexpectedly found that this inhibitor shows modest effects on HFD feeding-induced metabolic physiology, indicating that the beneficial role of MMP-12 knockdown did not rely on its enzymatic function. Unprecedentedly, both HFD feeding and FFA stimulation triggered a marked translocation of MMP-12 into the cell nucleus, as evidenced by IHC and immunocytochemistry (ICC) analyses. These results are in accordance with a previous study, which suggested that MMP-12 also exerts DNA-binding abilities [39] and thus functions as a transcriptional factor in response to virus infection. Similarly, in mouse small intestines, MMP-12 activates *FABP4* transcription by directly binding to the poly(A) tract presented on its proximal promoter. Histones respond sensitively to external signals, such as food and light, and thus undergo multiple posttranslational modifications, including acetylation and methylation [72,73]. However, the MMP-12-triggered epigenetic regulation of histones remains elusive. Our findings showed that overexpression of MMP-12 transformed the local chromatin environment of the poly(A) tract on the *FABP4* promoter into an active state, which was confirmed by increased ACh3 (an active biomarker) accumulation. However, we found that the levels of H3K9-me2 were not altered by MMP-12 overexpression. These results indicated that MMP-12 may function as an enhancer to facilitate gene transcription by altering histone acetylation rather than methylation. Hence, our findings extend the current recognition of the epigenetic regulation of lipid transportation and intestinal homeostasis via the MMP-12/FABP4 axis.

5. Conclusion

In conclusion, the present study highlights a non-classic transcriptional regulatory function of MMP-12 in mouse small intestines that activates *Fabp4* transcription to regulate the homeostasis of small intestinal homeostasis and whole-body metabolism. In addition, we established a small intestine-specific CPA NPs system, thus providing proof-of-concept siRNA-based metabolic gene manipulations. Translational research that advances the clinical applications of the CPA NPs system and therapeutic interventions targeting MMP-12 will benefit patients with obesity and its associated diseases.

Declaration of competing interest

The authors declare no competing financial interest.

Acknowledgments

This work was financially supported by grants from the National Natural Science Foundation of China (31800992, 92057112, 31771298 and 81800512), the Natural Science Foundation of Jiangsu Province (BK20180554 and BK20180577), the Project of State Key Laboratory of Natural Medicines, China Pharmaceutical University (SKLNMZZ202005), and the Priority Academic Program Development of Jiangsu Higher Education Institutions (PAPD).

Appendix A. Supplementary data

Supplementary data to this article can be found online at <https://doi.org/10.1016/j.biomaterials.2021.121183>.

Data availability

The data that support this study are available within the article and its supplementary data files or available from the authors upon request.

Credit author statement

MS, CL and SC conceived the project. MS, ZT, YS and YX performed the experiments. MS, SZ, WZ and SC wrote the manuscript, prepared the figures and was responsible for data compilation and integration. JL provided the clinical samples. All authors contributed significant feedback and additions. All authors have given approval to the final version of the manuscript.

References

- [1] B.A. Swinburn, V.I. Kraak, S. Allender, V.J. Atkins, P.I. Baker, J.R. Bogard, H. Brinsden, A. Calvillo, O. De Schutter, R. Devarajan, M. Ezzati, S. Friel, S. Goenka, R.A. Hammond, G. Hastings, C. Hawkes, M. Herrero, P.S. Howmand, M. Howden, L.M. Jaacks, A.B. Kapetanaki, M. Kasman, H.V. Kuhnlein, S. K. Kumanyika, B. Larjani, T. Lobstein, M.W. Long, V.K.R. Matsudo, S.D.H. Mills, G. Morgan, A. Morshed, P.M. Nece, A. Pan, D.W. Patterson, G. Sacks, M. Shekar, G. L. Simmons, W. Smit, A. Tootee, S. Vandevijvere, W.E. Waterlander, L. Wolfenden, W.H. Dietz, The global syndemic of obesity, undernutrition, and climate change: the lancet commission report, *Lancet* 393 (2019) 791–846, 10173.
- [2] L.K. Maresch, P. Benedikt, U. Feiler, S. Eder, K.A. Zierler, U. Taschler, S. Kolleritsch, T.O. Eichmann, G. Schoiswohl, C. Leopold, B.I. Wieser, C. Lackner, T. Rulicke, J. van Klinken, D. Kratky, T. Moustafa, G. Hoefler, G. Haemmerle, Intestine-specific overexpression of carboxylesterase 2c protects mice from diet-induced liver steatosis and obesity, *Hepatology* 3 (2) (2019) 227–245.
- [3] J. Upadhyay, O. Farr, N. Perakakis, W. Ghaly, C. Mantzoros, Obesity as a disease, *Med. Clin.* 102 (1) (2018) 13–33.
- [4] C.W. Ko, J. Qu, D.D. Black, P. Tso, Regulation of intestinal lipid metabolism: current concepts and relevance to disease, *Nat. Rev. Gastroenterol. Hepatol.* 17 (3) (2020) 169–183.
- [5] Y. Xu, M. Van Hul, F. Suriano, V. Preat, P.D. Cani, A. Belouqui, Novel strategy for oral peptide delivery in incretin-based diabetes treatment, *Gut* 69 (5) (2020) 911–919.
- [6] Y. Wan, F. Wang, J. Yuan, J. Li, D. Jiang, J. Zhang, H. Li, R. Wang, J. Tang, T. Huang, J. Zheng, A.J. Sinclair, J. Mann, D. Li, Effects of dietary fat on gut microbiota and faecal metabolites, and their relationship with cardiometabolic risk factors: a 6-month randomised controlled-feeding trial, *Gut* 68 (8) (2019) 1417–1429.
- [7] F. Kuipers, V.W. Bloks, A.K. Groen, Beyond intestinal soap–bile acids in metabolic control, *Nat. Rev. Endocrinol.* 10 (8) (2014) 488–498.
- [8] S.J. Alexopoulos, S.Y. Chen, A.E. Brandon, J.M. Salamoun, F.L. Byrne, C.J. Garcia, M. Beretta, E.M. Olzomer, D.P. Shah, A.M. Philp, S.R. Hargett, R.T. Lawrence, B. Lee, J. Sliagar, P. Carrive, S.P. Tucker, A. Philp, C. Lackner, N. Turner, G. J. Cooney, W.L. Santos, K.L. Hoehn, Mitochondrial uncoupler BAM15 reverses diet-induced obesity and insulin resistance in mice, *Nat. Commun.* 11 (1) (2020) 2397.
- [9] S. Shi, N. Kong, C. Feng, A. Shajii, C. Bejgrowicz, W. Tao, O.C. Farokhzad, Drug delivery strategies for the treatment of metabolic diseases, *Adv. Healthcare Mater.* 8 (12) (2019), e1801655.
- [10] Y. Zhang, J.R. Sowers, J. Ren, Targeting autophagy in obesity: from pathophysiology to management, *Nat. Rev. Endocrinol.* 14 (6) (2018) 356–376.
- [11] W. Wang, J. Zhao, W. Gui, D. Sun, H. Dai, L. Xiao, H. Chu, F. Du, Q. Zhu, B. Schnabl, K. Huang, L. Yang, X. Hou, Tauroursodeoxycholic acid inhibits intestinal inflammation and barrier disruption in mice with non-alcoholic fatty liver disease, *Br. J. Pharmacol.* 175 (3) (2018) 469–484.
- [12] H. Luo, M. Jiang, G. Lian, Q. Liu, M. Shi, T.Y. Li, L. Song, J. Ye, Y. He, L. Yao, C. Zhang, Z.Z. Lin, C.S. Zhang, T.J. Zhao, W.P. Jia, P. Li, S.Y. Lin, S.C. Lin, AIDA selectively mediates downregulation of fat synthesis enzymes by ERAD to retard intestinal fat absorption and prevent obesity, *Cell Metabol.* 27 (4) (2018) 843–853 e6.
- [13] L.G. Hersoug, P. Moller, S. Loft, Gut microbiota-derived lipopolysaccharide uptake and trafficking to adipose tissue: implications for inflammation and obesity, *Obes. Rev.* 17 (4) (2016) 297–312.
- [14] F. Zhang, G. Zarkada, J. Han, J. Li, A. Dubrac, R. Ola, G. Genet, K. Boye, P. Michon, S.E. Kunzel, J.P. Camporez, A.K. Singh, G.H. Fong, M. Simons, P. Tso, C. Fernandez-Hernando, G.I. Shulman, S.A. Sessa, A. Eichmann, Lactal junction zipper protects against diet-induced obesity, *Science* 361 (6402) (2018) 599–603.
- [15] C. Xiao, P. Stahel, A.L. Carreiro, K.K. Buhman, G.F. Lewis, Recent advances in triacylglycerol mobilization by the gut, *Trends Endocrinol. Metabol.* 29 (3) (2018) 151–163.
- [16] B. Wang, X. Rong, M.A. Duerr, D.J. Hermanson, P.N. Hedde, J.S. Wong, T. Q. Vallim, B.F. Cravatt, E. Gratton, D.A. Ford, P. Tontonoz, Intestinal phospholipid remodeling is required for dietary-lipid uptake and survival on a high-fat diet, *Cell Metabol.* 23 (3) (2016) 492–504.
- [17] A.T. Virtue, S.J. McCright, J.M. Wright, M.T. Jimenez, W.K. Mowel, J.J. Kotzkin, L. Joannas, M.G. Basavappa, S.P. Spencer, M.L. Clark, S.H. Eisenagel, A. Williams, M. Levy, S. Manne, S.E. Henrickson, E.J. Wherry, C.A. Thaiss, E. Elinav, J. Heno-Mejia, The gut microbiota regulates white adipose tissue inflammation and obesity via a family of microRNAs, *Sci. Transl. Med.* 11 (496) (2019).
- [18] K. Martinez-Guryn, N. Hubert, K. Frazier, S. Urras, M.W. Musch, P. Ojeda, J. F. Pierre, J. Miyoshi, T.J. Sontag, C.M. Cham, C.A. Reardon, V. Leone, E.B. Chang, Small intestine microbiota regulate host digestive and absorptive adaptive responses to dietary lipids, *Cell Host Microbe* 23 (4) (2018) 458–469, e5.
- [19] L. Garidou, C. Pomié, P. Klopp, A. Waget, J. Charpentier, M. Aloulou, A. Giry, M. Serino, L. Stenman, S. Lahtinen, C. Dray, Jason S. Iacovoni, M. Courtney, X. Collet, J. Amar, F. Servant, B. Lelouvier, P. Valet, G. Eberl, N. Fazilleau, V. Douin-Echinard, C. Heymes, R. Burcelin, The gut microbiota regulates intestinal CD4 T cells expressing ROR γ t and controls metabolic disease, *Cell Metabol.* 22 (1) (2015) 100–112.
- [20] A.R. Saltiel, J.M. Olefsky, Inflammatory mechanisms linking obesity and metabolic disease, *J. Clin. Invest.* 127 (1) (2017) 1–4.
- [21] C. Campbell, P.T. McKenney, D. Konstantinovskiy, O.I. Isaeva, M. Schizas, J. Verter, C. Mai, W.B. Jin, C.J. Guo, S. Violante, R.J. Ramos, J.R. Cross, K. Kadaveru, J. Hambor, A.Y. Rudensky, Bacterial metabolism of bile acids promotes generation of peripheral regulatory T cells, *Nature* 581 (7809) (2020) 475–479.
- [22] J.E. Hall, J.M. do Carmo, A.A. da Silva, Z. Wang, M.E. Hall, Obesity, kidney dysfunction and hypertension: mechanistic links, *Nat. Rev. Nephrol.* 15 (6) (2019) 367–385.
- [23] A. Dufour, C. Bellac, U. Eckhard, N. Solis, T. Klein, R. Kappelhoff, N. Fortelny, P. Jobin, J. Rozmus, J. Mark, P. Pavlidis, V. Dive, S. Barbour, C. Overall, C-terminal truncation of IFN- γ inhibits proinflammatory macrophage responses and is deficient in autoimmune disease, *Nat. Commun.* 9 (1) (2018) 2416.
- [24] V. Lagente, C. Le Qument, E. Boichot, Macrophage metalloelastase (MMP-12) as a target for inflammatory respiratory diseases, *Expert Opin. Ther. Targets* 13 (3) (2009) 287–295.
- [25] Y.E. Koshman, N. Patel, M. Chu, R. Iyengar, T. Kim, C. Ersahin, W. Lewis, A. Heroux, A.M. Samarel, Regulation of connective tissue growth factor gene expression and fibrosis in human heart failure, *J. Card. Fail.* 19 (4) (2013) 283–294.
- [26] M. Zha, T. Tian, W. Xu, S. Liu, J. Jia, L. Wang, Q. Yan, N. Li, J. Yu, L. Huang, The circadian clock gene Bmal1 facilitates cisplatin-induced renal injury and hepatization, *Cell Death Dis.* 11 (6) (2020) 446.
- [27] S. Chen, M. Feng, S. Zhang, Z. Dong, Y. Wang, W. Zhang, C. Liu, Angptl8 mediates food-driven resetting of hepatic circadian clock in mice, *Nat. Commun.* 10 (1) (2019) 3518.
- [28] X. Shan, L. Tomlinson, Q. Yang, H. Colognato, Distinct requirements for extracellular and intracellular MMP12 in the development of the adult V-SVZ neural stem cell niche, *Stem Cell Rep.* 10 (3) (2018) 984–999.
- [29] C. Risanayanti, Y.S. Jang, J. Lee, H.J. Ahn, PLGA nanoparticles co-delivering MDR1 and BCL2 siRNA for overcoming resistance of paclitaxel and cisplatin in recurrent and advanced ovarian cancer, *Sci. Rep.* 8 (1) (2018) 7498.
- [30] S. Xiang, M. Sarem, S. Shah, V.P. Shastri, Liposomal treatment of cancer cells modulates uptake pathway of polymeric nanoparticles by altering membrane stiffness, *Small* 14 (14) (2018).
- [31] F. He, Y. Huang, Z. Song, H.J. Zhou, H. Zhang, R.J. Perry, G.I. Shulman, W. Min, Mitophagy-mediated adipose inflammation contributes to type 2 diabetes with hepatic insulin resistance, *J. Exp. Med.* 218 (3) (2021).
- [32] Z. Liu, X. Dai, H. Zhang, R. Shi, Y. Hui, X. Jin, W. Zhang, L. Wang, Q. Wang, D. Wang, J. Wang, X. Tan, B. Ren, X. Liu, T. Zhao, J. Wang, J. Pan, T. Yuan, C. Chu, L. Lan, F. Yin, E. Cadenas, L. Shi, S. Zhao, X. Liu, Gut microbiota mediates intermittent-fasting alleviation of diabetes-induced cognitive impairment, *Nat. Commun.* 11 (1) (2020).
- [33] W. Zhang, Z. Dong, M. Xu, S. Zhang, C. Liu, S. Chen, SWI/SNF complex subunit BAF60a represses hepatic ureagenesis through a crosstalk between YB-1 and PGC-1 α , *Mol. Metabol.* 32 (2020) 85–96.
- [34] W.J. Yan, B.Y. Zhang, M.P. Yadav, L.P. Feng, J.X. Yan, X. Jia, L.J. Yin, Corn fiber gum-soybean protein isolate double network hydrogel as oral delivery vehicles for thermosensitive bioactive compounds, *Food Hydrocolloids* 107 (2020).
- [35] M.A. Islam, Y. Xu, W. Tao, J.M. Ubellacker, M. Lim, D. Aum, G.Y. Lee, K. Zhou, H. Zope, M. Yu, W. Cao, J.T. Oswald, M. Dinarvand, M. Mahmoudi, R. Langer, P. W. Kantoff, O.C. Farokhzad, B.R. Zetter, J. Shi, Restoration of tumour-growth suppression in vivo via systemic nanoparticle-mediated delivery of PTEN mRNA, *Nat. Biomed. Eng.* 2 (11) (2018) 850–864.
- [36] R.W. O'Rourke, Inflammation in obesity-related diseases, *Surgery* 145 (3) (2009) 255–259.
- [37] M. Monteiro-Sepulveda, S. Touch, C. Mendes-Sa, S. Andre, C. Poitou, O. Allatif, A. Cottillard, H. Fohrer-Ting, E.L. Hubert, R. Remark, L. Genser, J. Tordjman, K. Garbin, C. Osinski, C. Sautes-Fridman, A. Leturque, K. Clement, E. Brot-Laroche, Jejunal T cell inflammation in human obesity correlates with decreased enterocyte insulin signaling, *Cell Metabol.* 22 (1) (2015) 113–124.
- [38] P. Clancy, S.W. Seto, S.A. Koblar, J. Golledge, Role of the angiotensin converting enzyme 1/angiotensin II/angiotensin receptor 1 axis in interstitial collagenase expression in human carotid atherosclerosis, *Atherosclerosis* 229 (2) (2013) 331–337.
- [39] D.J. Marchant, C.L. Bellac, T.J. Moraes, S.J. Wadsworth, A. Dufour, G.S. Butler, L. M. Bilawchuk, R.G. Hendry, A.G. Robertson, C.T. Cheung, J. Ng, L. Ang, Z. Luo, K. Heilbron, M.J. Norris, W. Duan, T. Bucyk, A. Karpov, L. Devel, D. Georgiadis, R. G. Hegele, H. Luo, D.J. Granville, V. Dive, B.M. McManus, C.M. Overall, A new transcriptional role for matrix metalloproteinase-12 in antiviral immunity, *Nat. Med.* 20 (5) (2014) 493–502.
- [40] B. Li, J. Hao, J. Zeng, E.R. Sauter, SnapShot: FABP functions, *Cell* 182 (4) (2020) 1066–1066 e1.

- [41] G.S. Hotamisligil, D.A. Bernlohr, Metabolic functions of FABPs—mechanisms and therapeutic implications, *Nat. Rev. Endocrinol.* 11 (10) (2015) 592–605.
- [42] K.N. Charles, M.D. Li, F. Engin, A.P. Arruda, K. Inouye, G.S. Hotamisligil, Uncoupling of metabolic health from longevity through genetic alteration of adipose tissue lipid-binding proteins, *Cell Rep.* 21 (2) (2017) 393–402.
- [43] S. Lattanzi, M. Di Napoli, S. Ricci, A.A. Divani, Matrix metalloproteinases in acute intracerebral hemorrhage, *Neurotherapeutics* 17 (2) (2020) 484–496.
- [44] Y. Ren, H.W. Cheung, G. von Maltzhan, A. Agrawal, G.S. Cowley, B.A. Weir, J. S. Boehm, P. Tamayo, A.M. Karst, J.F. Liu, M.S. Hirsch, J.P. Mesirov, R. Drapkin, D. E. Root, J. Lo, V. Fogal, E. Ruoslahti, W.C. Hahn, S.N. Bhatia, Targeted tumor-penetrating siRNA nanocomplexes for credentialing the ovarian cancer oncogene ID4, *Sci. Transl. Med.* 4 (147) (2012), 147ra112.
- [45] K.Y. Choi, S. Correa, J. Min, J. Li, S. Roy, K.H. Laccetti, E. Dreaden, S. Kong, R. Heo, Y.H. Roh, E.C. Lawson, P.A. Palmer, P.T. Hammond, Binary targeting of siRNA to hematologic cancer cells in vivo using layer-by-layer nanoparticles, *Adv. Funct. Mater.* 29 (20) (2019).
- [46] R. Kanasty, J.R. Dorkin, A. Vegas, D. Anderson, Delivery materials for siRNA therapeutics, *Nat. Mater.* 12 (11) (2013) 967–977.
- [47] H.H. Guo, C. Ma, W.S. Zheng, Y. Luo, C. Li, X.L. Li, X.L. Ma, C.L. Feng, T.T. Zhang, Y.X. Han, Z.G. Luo, Y. Zhan, R. Li, L.L. Wang, J.D. Jiang, Dual-stimuli-responsive gut microbiota-targeting berberine-CS/PT-NPs improved metabolic status in obese hamsters, *Adv. Funct. Mater.* 29 (14) (2019).
- [48] Y. Xue, X. Xu, X.Q. Zhang, O.C. Farokhzad, R. Langer, Preventing diet-induced obesity in mice by adipose tissue transformation and angiogenesis using targeted nanoparticles, *Proc. Natl. Acad. Sci. U. S. A.* 113 (20) (2016) 5552–5557.
- [49] Y. Shi, J. Xue, L. Jia, Q. Du, J. Niu, D. Zhang, Surface-modified PLGA nanoparticles with chitosan for oral delivery of tolbutamide, *Colloids Surf. B Biointerfaces* 161 (2018) 67–72.
- [50] B. Menchicchi, J.P. Fuenzalida, K.B. Bobbili, A. Hensel, M.J. Swamy, F. M. Goycoolea, Structure of chitosan determines its interactions with mucin, *Biomacromolecules* 15 (10) (2014) 3550–3558.
- [51] J. He, Y. Song, G. Li, P. Xiao, Y. Liu, Y. Xue, Q. Cao, X. Tu, T. Pan, Z. Jiang, X. Cao, L. Lai, Q. Wang, Fbxw7 increases CCL2/7 in CX3CR1hi macrophages to promote intestinal inflammation, *J. Clin. Invest.* 129 (9) (2019) 3877–3893.
- [52] R. Smith, R. Jones, U. Specks, S. Bond, M. Nodale, R. Aljayyousi, J. Andrews, A. Bruchfeld, B. Camilleri, S. Carette, C. Cheung, V. Derebail, T. Doulton, L. Forbess, S. Fujimoto, S. Furuta, O. Gewurz-Singer, L. Harper, T. Ito-Ihara, N. Khalidi, R. Klocke, C. Koenig, Y. Komagata, C. Langford, P. Lanyon, R. Luqmani, H. Makino, C. McAlear, P. Monach, L. Moreland, K. Mynard, P. Nachman, C. Pagnoux, F. Pearce, C. Peh, C. Pusey, D. Ranganathan, R. Rhee, R. Spiera, A. Sreih, V. Tesar, G. Walters, M. Weisman, C. Wroe, P. Merkel, D. Jayne, Rituximab as therapy to induce remission after relapse in ANCA-associated vasculitis, *Ann. Rheum. Dis.* 79 (9) (2020) 1243–1249.
- [53] D.L. Lavery, P. Martinez, L.J. Gay, B. Cereser, M.R. Novelli, M. Rodriguez-Justo, S. L. Meijer, T.A. Graham, S.A. McDonald, N.A. Wright, M. Jansen, Evolution of oesophageal adenocarcinoma from metaplastic columnar epithelium without goblet cells in Barrett's oesophagus, *Gut* 65 (6) (2016) 907–913.
- [54] W.S. Garrett, J.I. Gordon, L.H. Glimcher, Homeostasis and inflammation in the intestine, *Cell* 140 (6) (2010) 859–870.
- [55] N. Fuke, N. Nagata, H. Suganuma, T. Ota, Regulation of gut microbiota and metabolic endotoxemia with dietary factors, *Nutrients* 11 (10) (2019).
- [56] Q. Li, Z. Cheng, L. Zhou, S. Darmanis, N. Neff, J. Okamoto, G. Gulati, M. Bennett, L. Sun, L. Clarke, J. Marschallinger, G. Yu, S. Quake, T. Wyss-Coray, B. Barres, Developmental heterogeneity of microglia and brain myeloid cells revealed by deep single-cell RNA sequencing, *Neuron* 101 (2) (2019) 207–223, e10.
- [57] F. Biase, X. Cao, S. Zhong, Cell fate inclination within 2-cell and 4-cell mouse embryos revealed by single-cell RNA sequencing, *Genome Res.* 24 (11) (2014) 1787–1796.
- [58] Q. Ni, F. Zhang, Y. Liu, Z. Wang, G. Yu, B. Liang, G. Niu, T. Su, G. Zhu, G. Lu, L. Zhang, X. Chen, A bi-adjuvant nanovaccine that potentiates immunogenicity of neoantigen for combination immunotherapy of colorectal cancer, *Sci. Adv.* 6 (12) (2020), eaaw6071.
- [59] B. Manoury, S. Nenan, I. Guenon, E. Boichot, J.M. Planquois, C.P. Bertrand, V. Lagente, Macrophage metalloelastase (MMP-12) deficiency does not alter bleomycin-induced pulmonary fibrosis in mice, *J. Inflamm.* 3 (2006) 2.
- [60] J.T. Lee, N. Pamir, N.C. Liu, E.A. Kirk, M.M. Averill, L. Becker, I. Larson, D. K. Hagman, K.E. Foster-Schubert, B. van Yserloo, K.E. Bornfeldt, R.C. LeBoeuf, M. Kratz, J.W. Heinecke, Macrophage metalloelastase (MMP12) regulates adipose tissue expansion, insulin sensitivity, and expression of inducible nitric oxide synthase, *Endocrinology* 155 (9) (2014) 3409–3420.
- [61] B. Marcheva, K. Ramsey, E. Buhr, Y. Kobayashi, H. Su, C. Ko, G. Ivanova, C. Omura, S. Mo, M. Vitaterna, J. Lopez, L. Philipson, C. Bradfield, S. Crosby, L. JeBailey, X. Wang, J. Takahashi, J. Bass, Disruption of the clock components CLOCK and BMAL1 leads to hypoinsulinaemia and diabetes, *Nature* 466 (7306) (2010) 627–631.
- [62] K.A. Lamia, K.F. Storch, C.J. Weitz, Physiological significance of a peripheral tissue circadian clock, *Proc. Natl. Acad. Sci. U. S. A.* 105 (39) (2008) 15172–15177.
- [63] X. Su, H. Yan, Y. Huang, H. Yun, B. Zeng, E. Wang, Y. Liu, Y. Zhang, F. Liu, Y. Che, Z. Zhang, R. Yang, Expression of FABP4, adipin and adiponectin in Paneth cells is modulated by gut Lactobacillus, *Sci. Rep.* 5 (2015) 18588.
- [64] M. Aristorena, E. Gallardo-Vara, M. Vicen, M. de Las Casas-Engel, L. Ojeda-Fernandez, C. Nieto, F.J. Blanco, A.C. Valbuena-Diez, L.M. Botella, P. Nachtigal, MMP-12, secreted by pro-inflammatory macrophages, targets endoglin in human macrophages and endothelial cells, *Int. J. Mol. Sci.* 20 (12) (2019) 3107.
- [65] H. Song, X. Shen, R. Deng, Y. Zhang, X. Zheng, Dietary anthocyanin-rich extract of açai protects from diet-induced obesity, liver steatosis, and insulin resistance with modulation of gut microbiota in mice, *Nutrition* 86 (2021) 111176.
- [66] Y. Qiao, L. Liu, L. Yin, L. Xu, Z. Tang, Y. Qi, Z. Mao, Y. Zhao, X. Ma, J. Peng, FABP4 contributes to renal interstitial fibrosis via mediating inflammation and lipid metabolism, *Cell Death Dis.* 10 (6) (2019) 382.
- [67] K. Maeda, H. Cao, K. Kono, C.Z. Gorgun, M. Furuhashi, K.T. Uysal, Q. Cao, G. Atsumi, H. Malone, B. Krishnan, Y. Minokoshi, B.B. Kahn, R.A. Parker, G. S. Hotamisligil, Adipocyte/macrophage fatty acid binding proteins control integrated metabolic responses in obesity and diabetes, *Cell Metabol.* 1 (2) (2005) 107–119.
- [68] Y. Zhang, Q. Li, E. Rao, Y. Sun, M.E. Grossmann, R.J. Morris, M.P. Cleary, B. Li, Epidermal Fatty Acid binding protein promotes skin inflammation induced by high-fat diet, *Immunity* 42 (5) (2015) 953–964.
- [69] J.W. Li, B. Fang, G.F. Pang, M. Zhang, F.Z. Ren, Age- and diet-specific effects of chronic exposure to chlorpyrifos on hormones, inflammation and gut microbiota in rats, *Pestic. Biochem. Physiol.* 159 (2019) 68–79.
- [70] B. Meissburger, L. Stachorski, E. Roder, G. Rudofsky, C. Wolftrum, Tissue inhibitor of matrix metalloproteinase 1 (TIMP1) controls adipogenesis in obesity in mice and in humans, *Diabetologia* 54 (6) (2011) 1468–1479.
- [71] A.L. Strong, J.A. Semon, T.A. Strong, T.T. Santoko, S. Zhang, H.E. McFerrin, J. M. Gimble, B.A. Bunnell, Obesity-associated dysregulation of calpastatin and MMP-15 in adipose-derived stromal cells results in their enhanced invasion, *Stem Cell.* 30 (12) (2012) 2774–2783.
- [72] S.L. Berger, An embarrassment of niches: the many covalent modifications of histones in transcriptional regulation, *Oncogene* 20 (24) (2001) 3007–3013.
- [73] B.D. Strahl, C.D. Allis, The language of covalent histone modifications, *Nature* 403 (6765) (2000) 41–45.